Article

Immunity

MHC Class II Antigen Presentation by the Intestinal Epithelium Initiates Graft-versus-Host Disease and Is Influenced by the Microbiota

Graphical Abstract

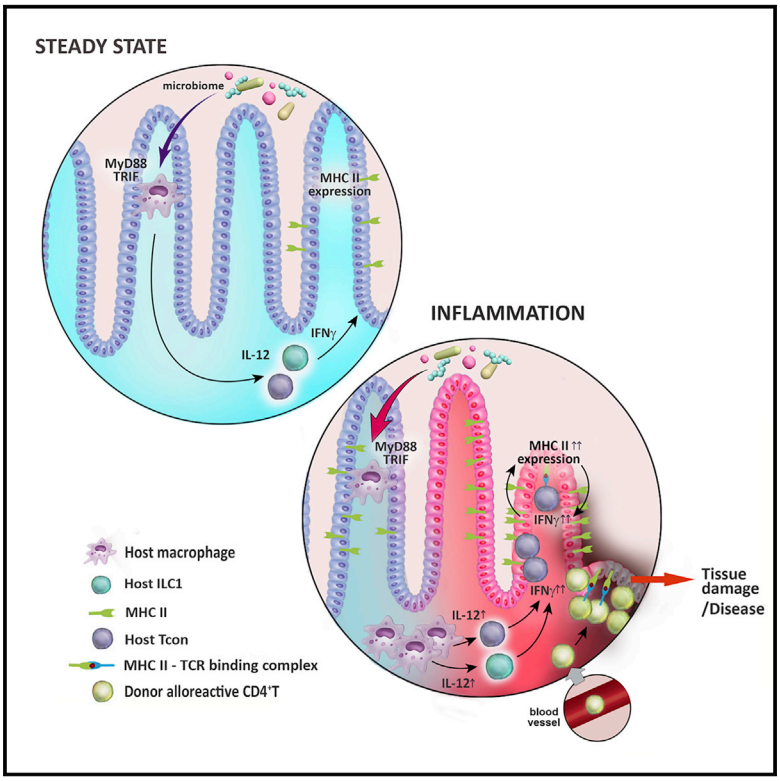

Highlights

- The microbiota influences MHC class II expression on IECs in the ileum
- MHC class II expression on IECs requires an IL-12-IFNγ cytokine axis
- MHC class II$^+$ IECs present antigen, activate CD4$^+$ T cells, and initiate lethal gut GVHD
- IL-12/23p40 neutralization pretransplant prevents the initiation of lethal GVHD

Authors

Motoko Koyama,
Pamela Mukhopadhyay,
Iona S. Schuster, ...,
Andrew D. Clouston,
Mariapia A. Degli-Esposti,
Geoffrey R. Hill

Correspondence

mkoyama@fredhutch.org (M.K.),
grhill@fredhutch.org (G.R.H.)

In Brief

Graft-versus-host disease in the gastrointestinal tract is the principal determinant of lethality following allogeneic bone marrow transplantation. Koyama et al. find that MHC class II-dependent antigen presentation by ileal intestinal epithelial cells (IECs) is critical for the initiation of lethal GVHD in the gut, define the requirements for IEC MHC class II expression, and propose IL-12 neutralization as a therapeutic strategy for GVHD.

Koyama et al., 2019, Immunity *51*, 885–898
November 19, 2019
https://doi.org/10.1016/j.immuni.2019.08.011

CellPress

Immunity
Article

MHC Class II Antigen Presentation by the Intestinal Epithelium Initiates Graft-versus-Host Disease and Is Influenced by the Microbiota

Motoko Koyama,[1,15,*] Pamela Mukhopadhyay,[2] Iona S. Schuster,[3,4,5] Andrea S. Henden,[1,6] Jan Hülsdünker,[7,8,9] Antiopi Varelias,[1] Marie Vetizou,[10] Rachel D. Kuns,[1] Renee J. Robb,[1] Ping Zhang,[1] Bruce R. Blazar,[11] Ranjeny Thomas,[12] Jakob Begun,[13] Nicola Waddell,[2] Giorgio Trinchieri,[10] Robert Zeiser,[7] Andrew D. Clouston,[14] Mariapia A. Degli-Esposti,[3,4,5] and Geoffrey R. Hill[1,6,15,16,17,*]

[1]Bone Marrow Transplantation Laboratory, Immunology Department, QIMR Berghofer Medical Research Institute, Brisbane, QLD 4006, Australia
[2]Medical Genomics Laboratory, Genetics and Computational Biology Department, QIMR Berghofer Medical Research Institute, Brisbane, QLD 4006, Australia
[3]Immunology and Virology Program, Centre for Ophthalmology and Visual Science, The University of Western Australia, Crawley, WA 6009, Australia
[4]Centre for Experimental Immunology, Lions Eye Institute, Nedlands, WA 6009, Australia
[5]Infection and Immunity Program and Department of Microbiology, Biomedicine Discovery Institute, Monash University, Clayton, VIC 3800, Australia
[6]Department of Haematology and Bone Marrow Transplantation, Cancer Care Services, Royal Brisbane and Women's Hospital, Brisbane, QLD 4029, Australia
[7]Department of Hematology, Oncology and Stem Cell Transplantation, Freiburg University Medical Center, Albert Ludwigs University Freiburg, Freiburg 79106, Germany
[8]Spemann Graduate School of Biology and Medicine, University Freiburg, Freiburg 79085, Germany
[9]Faculty of Biology, University Freiburg, Freiburg 79104, Germany
[10]Cancer and Inflammation Program, Center for Cancer Research, NCI, NIH, Bethesda, MD 20892, USA
[11]Division of Blood and Marrow Transplantation, Department of Pediatrics, University of Minnesota, Minneapolis, MN 55455, USA
[12]Diamantina Institute, Translational Research Institute, University of Queensland, Princess Alexandra Hospital, Brisbane, QLD 4102, Australia
[13]Mater Research Institute, University of Queensland, Translational Research Institute, Brisbane, QLD 4102, Australia
[14]Envoi Specialist Pathologists, Brisbane, QLD 4006, Australia
[15]Clinical Research Division, Fred Hutchinson Cancer Research Center, Seattle, WA 98109, USA
[16]Division of Medical Oncology, University of Washington, Seattle, WA 98109, USA
[17]Lead Contact
*Correspondence: mkoyama@fredhutch.org (M.K.), grhill@fredhutch.org (G.R.H.)
https://doi.org/10.1016/j.immuni.2019.08.011

SUMMARY

Graft-versus-host disease (GVHD) in the gastrointestinal (GI) tract is the principal determinant of lethality following allogeneic bone marrow transplantation (BMT). Here, we examined the mechanisms that initiate GVHD, including the relevant antigen-presenting cells. MHC class II was expressed on intestinal epithelial cells (IECs) within the ileum at steady state but was absent from the IECs of germ-free mice. IEC-specific deletion of MHC class II prevented the initiation of lethal GVHD in the GI tract. MHC class II expression on IECs was absent from mice deficient in the TLR adaptors MyD88 and TRIF and required IFNγ secretion by lamina propria lymphocytes. IFNγ responses are characteristically driven by IL-12 secretion from myeloid cells. Antibiotic-mediated depletion of the microbiota inhibited IL-12/23p40 production by ileal macrophages. IL-12/23p40 neutralization prevented MHC class II upregulation on IECs and initiation of lethal GVHD in the GI tract. Thus, MHC class II expression by IECs in the ileum initiates lethal GVHD, and blockade of IL-12/23p40 may represent a readily translatable therapeutic strategy.

INTRODUCTION

The principal function of the immune system is to respond to pathogens in a timely and appropriate manner. This requires a balance of tightly regulated responses, especially at barrier sites such as the skin and the gastrointestinal (GI) tract, which are continuously exposed to microbial and environmental challenges. The GI tract plays a critical role in many inflammatory conditions, including graft-versus-host disease (GVHD) following allogeneic bone marrow transplantation (BMT). Acute GVHD of the GI tract, the prima facie determinant of disease severity and lethality (Hill and Ferrara, 2000), is the manifestation of immunopathology mediated by donor T cells (Zeiser and Blazar, 2017) in response to alloantigen presented by major histocompatibility complex (MHC) class I and MHC class II on antigen-presenting cells

(APCs) (Koyama and Hill, 2016; Shlomchik et al., 1999). In many settings, MHC class II-dependent responses are initiated by "professional" hematopoietic-derived APCs, including dendritic cells (DCs), macrophages, monocytes, and B cells (Kambayashi and Laufer, 2014; Unanue et al., 2016), but whether this is the case in GVHD is unclear. Non-hematopoietic cells, including mesenchymal cells and epithelial cells, can also express MHC class II when stimulated with interferon-γ (IFNγ) (Londei et al., 1984; McDonald and Jewell, 1987; Skoskiewicz et al., 1985); however, the physiological and pathological relevance of non-hematopoietic MHC class II expression and the relative importance of hematopoietic versus non-hematopoietic APC populations in GI inflammation during GVHD are largely undefined.

Damage to the GI tract plays a major role in the initiation and amplification of systemic inflammation and subsequent GVHD, and fatal GVHD is almost always a consequence of GI tract involvement (Ferrara et al., 2009). The role of the microbiota in altering the severity of GVHD has been noted. Intensive antibiotic-mediated gut decontamination attenuates acute GVHD and improves survival in clinical settings, including phase III randomized studies (Beelen et al., 1999; Vossen et al., 1990). Furthermore, qualitative changes in the microbiota, particularly the loss of microbiota diversity characterized by depletion of short-chain fatty acid-producing anaerobes, have been associated with impaired transplant outcome (Andermann et al., 2018; Mathewson et al., 2016). Thus, distinct protective and pathogenic components of the microbiota affect GVHD and survival following BMT.

In this study, we investigated how immune responses and pathology are regulated in the GI tract in the context of allogeneic BMT, a common clinical procedure that offers a curative therapy for most hematological malignancies. We focused on understanding the mechanisms controlling expression of MHC class II, because GVHD pathology is associated with $CD4^+$ T cell activity. We found that at steady state, intestinal epithelial cells (IECs) in the small intestine expressed MHC class II but that MHC class II expression was absent from IECs from germ-free mice. Maximal MHC class II expression on IECs required the expression of the Toll-like receptor (TLR) signaling adaptors MyD88 and TRIF in both hematopoietic and non-hematopoietic cells, suggesting a role for microbiota-derived TLR ligands. MHC class II expression was also regulated by cytokine signals: IL-12/23p40 from macrophages and IFNγ from lamina propria lymphocytes, including type 1 innate lymphoid cells (ILC1) and T cells. MHC class II expression on IECs increased after total body irradiation (TBI), which precedes graft transfer, concomitant with severe immunopathology in the GI tract. IEC-specific deletion of MHC class II abrogated gut pathology and lethal GVHD. Abrogation of GVHD lethality was also achieved by preventing MHC class II expression on IECs via IL-12/23p40 neutralization pretransplant. Our findings thus define cellular and molecular pathways that initiate GVHD in the GI tract and argue for IL-12/23p40 neutralization pretransplant as a potential therapeutic approach that can be readily tested in clinical settings.

RESULTS

IECs in the Ileum Express MHC Class II

The factors initiating immune pathology upon GVHD in the GI tract are unclear, including the relevant antigen-presenting cell. We thus undertook an analysis of MHC class II expression in various cells and anatomical sites of the GI tract by flow cytometric analysis. MHC class II was highly and preferentially expressed in the small intestine at steady state (Figures 1A and 1B). A large fraction of the non-hematopoietic MHC class II-expressing cells consisted of $Villin^+$ IECs. We then examined MHC class II expression within 4 days of BMT. Expression of MHC class II increased in the small intestine and, to a lesser extent, in the colon (Figures 1A and 1B). Within the small intestine, IECs in the ileum expressed higher amounts of MHC class II than the jejunum (Figure 1C). Confocal microscopy of the ileum of mice expressing GFP under the control of the $I\text{-}A^b\beta$ promoter revealed increased MHC class II transcription after conditioning with TBI (Figure 1D). The distribution of MHC class II GFP^+ cells overlapped with that of MHC class II antibody (Ab)-stained cells (Figure S1A).

The differential distribution of MHC class II in various sections of the GI tract suggested that there may be tissue site-specific differences that dictate IEC responses. We compared the depth of the inner mucous layer of the colon before and early after TBI, the conditioning that precedes transplantation, by confocal microscopy. We found that the inner mucous layer that shields IECs from bacteria remained intact in the first days following TBI (Figure 1E; Figure S1B). The mucous layer in the small intestine was less dense than the colonic inner mucous layer (Figure 1E), consistent with it being more permeable to small molecules (Shan et al., 2013). Concurrent staining of bacteria in the ileum of mice after TBI with a fluorescent *in situ* hybridization probe revealed that bacteria were present just above the villi, in direct contact with the IECs of the ileum, where an inner mucous layer was absent (Figure 1E). These findings suggest that the terminal ileum is a preferential site of mucosal-microbiota interaction, afforded at least partly by the presence of a limited mucous layer relative to that of the colon. This is consistent with data demonstrating translocation of bacteria, as determined by 16 s rRNA sequencing, preferentially in the ileum (Hülsdünker et al., 2018).

MHC Class II Expression by IECs in the Small Intestine Requires the Microbiota

Next, we investigated the role of the microbiota in driving MHC class II expression by IECs. We could not detect MHC class II expression on the IECs ($CD45^{neg}$ epithelial cell adhesion molecule $[EpCAM]^+$) of germ-free mice, even after TBI (Figures 2A–2C; Figure S1C). In contrast, MHC class II expression by hematopoietic APCs was intact in these animals and increased after TBI (Figure 2B). In a separate approach, we treated wild-type (WT) mice with broad-spectrum oral antibiotics (vancomycin, gentamicin, metronidazole, and cefoxitin) for 2 weeks and analyzed MHC class II expression in the GI tract thereafter. Depletion of the bacterial microbiota abrogated MHC class II expression on ileal IECs and prevented increased MHC class II expression on these cells after TBI, but it had no impact on hematopoietic APC MHC class II expression (Figures 2D and 2E; Figure S1D).

In mouse models, GVHD lethality is exacerbated by dysbiosis (Varelias et al., 2017). We asked whether MHC class II expression on IECs changed under conditions of dysbiosis. WT mice were rendered dysbiotic by cohousing with $Il17ra^{-/-}$ mice, as previously described (Varelias et al., 2017). Flow cytometric analysis revealed increased MHC class II expression by IECs in these

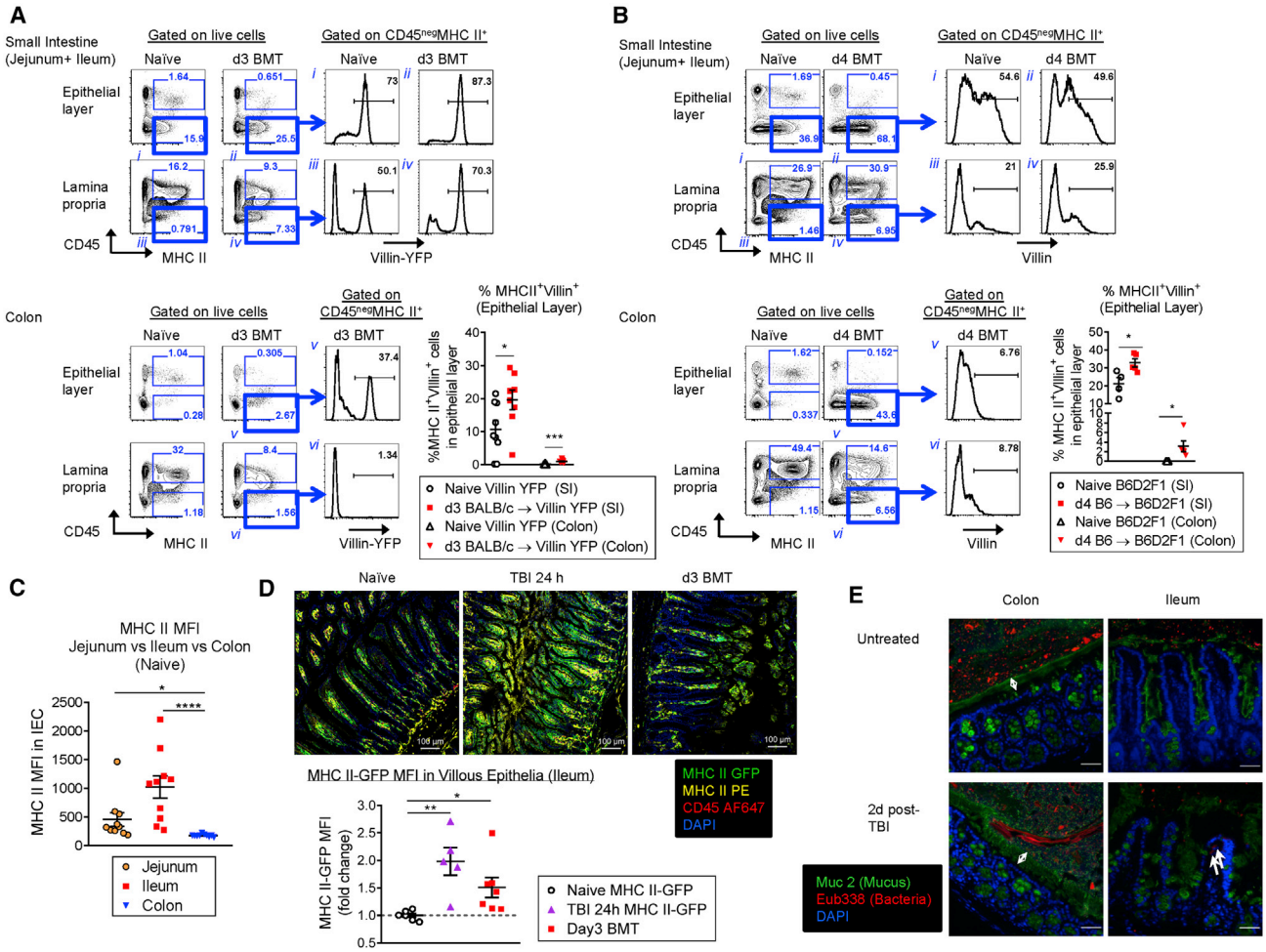

Figure 1. IECs in the Ileum Express MHC Class II, and MHC Class II Expression Increases after TBI

(A and B) MHC class II expression in the small intestine (pooled jejunum and ileum) and large intestine was analyzed in naive and transplanted mice. Representative flow plots and enumeration are shown.

(A) Lethally irradiated *Villin*Cre^{pos}*Rosa26*-YFP mice were transplanted with BM and T cells from BALB/c mice and analyzed on day 3 post-transplant. Data combined from 3 replicate experiments (n = 9 per group).

(B) Irradiated B6D2F1 mice were transplanted with BM and T cells from B6.WT mice and analyzed on day 4. Data combined from 2 replicate experiments (n = 4–5 per group).

(C) MHC class II expression (mean fluorescence intensity [MFI]) was quantified on IECs (EpCAM$^+$CD45^{neg}) of the jejunum, ileum, and colon from naive B6.WT mice. Data combined from 2 replicate experiments (n = 10 per group).

(D) Naive B6.*I-A$^b\beta$*-GFP mice 24 h after TBI or day 3 after BMT with BM and T cells from BALB/c mice as in (A). Immunofluorescence (green, MHC class II-GFP; yellow, MHC class II [anti-IA/IE Ab staining]; red, CD45; blue, DAPI). Representative images and standardized enumeration combined from 3 replicate experiments (n = 5–6 per group).

(E) Immunofluorescence staining of colonic and ileal tissue of naive B6 mice and at day 2 post-TBI. Bidirectional arrows indicate the colon's inner mucous layer, which is free from bacteria (Muc2, green; eubacterial probe [Eub338], red; DAPI, blue; scale bar, 50 μm). Single arrows demonstrate bacteria within the lamina propria.

Statistical analysis by unpaired t test per organ (A), Mann-Whitney U test per organ (B), or Kruskal-Wallis test (C and D) (mean ± SEM). *p < 0.05, **p < 0.01, ***p < 0.001.

See also Figure S1.

mice (Figures 2F and 2G), as well as increased donor CD4$^+$ T cell expansion after BMT, compared with WT mice that had not been rendered dysbiotic by prior co-housing (Figure 2H). Thus, MHC class II expression on IECs at steady state and upon inflammation requires the microbiota, and dysbiosis in a BMT setting is associated with increased IEC MHC class II expression and increased proliferation of pathogenic donor CD4$^+$ T cells after BMT.

MyD88 and TRIF Signaling Are Necessary for MHC Class II Expression by IECs

We then asked whether MHC class II on IECs could promote the activation and proliferation of naive CD4$^+$ T cells using an HY male antigen-specific T cell receptor (TCR) transgenic system (Marilyn T cells that recognize male peptide complexed within I-A^b) (Lantz et al., 2000). We cocultured sort-purified IECs collected from female or male mice 20 h after TBI with

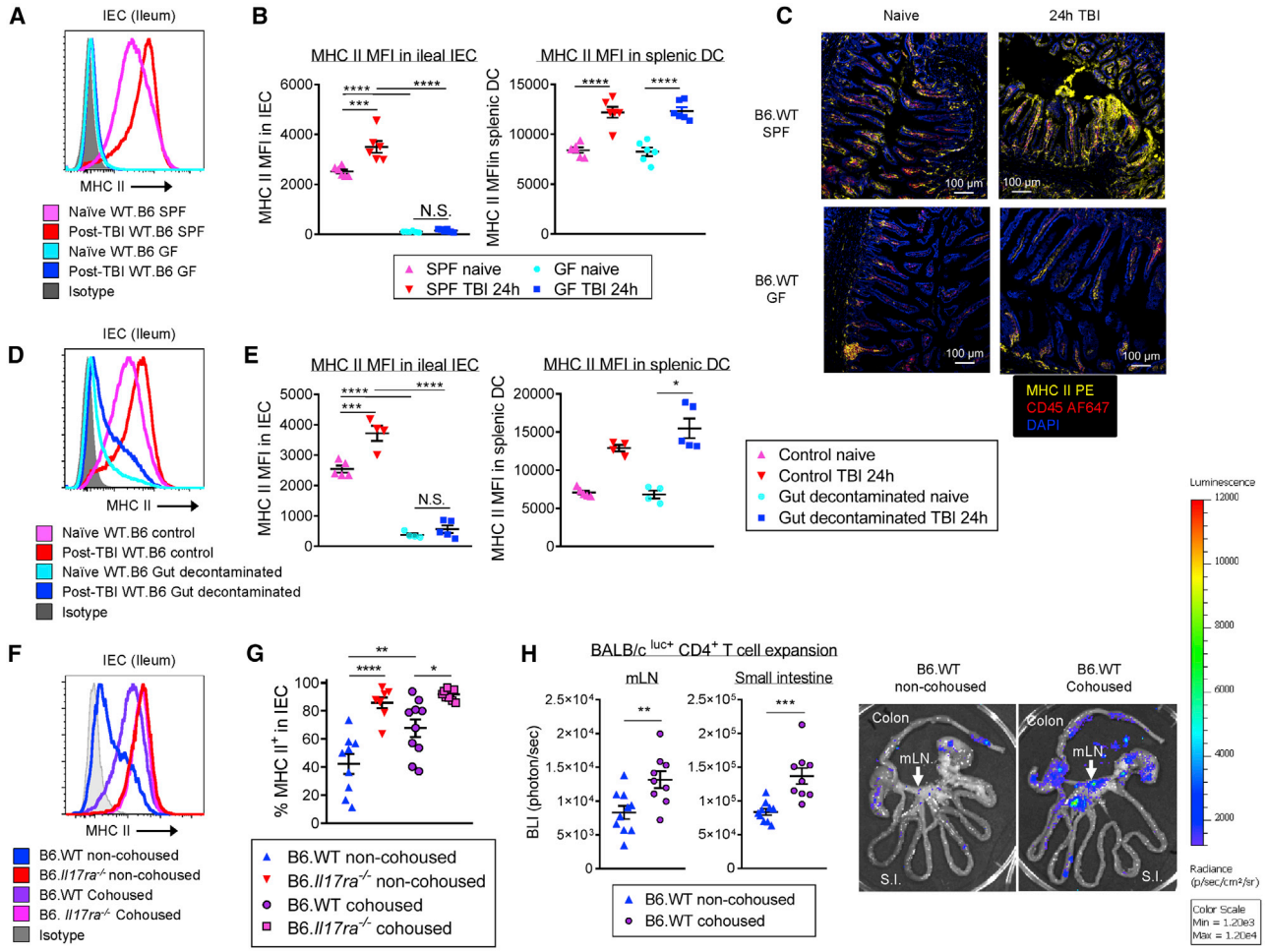

Figure 2. The Intestinal Microbiota Is Required for MHC Class II Expression on IEC Pretransplant

(A) Representative histograms of MHC class II on ileal IECs (EpCAM$^+$CD45^{neg}) purified from specific pathogen-free (SPF) and germ-free (GF) mice before (naive) and 24 h after TBI.

(B) MHC class II MFI on IECs and splenic DCs (CD45$^+$CD3^{neg}CD19^{neg}NK1.1^{neg}Ly6C^{neg}Ly6G^{neg}CD11c$^+$CD64^{neg}) (n = 6 per group from 3 experiments).

(C) Confocal images from the ileum.

(D and E) Mice were treated with antibiotic water or control water for 2 weeks and analyzed before (naive) and 24 h after TBI. Representative histograms of MHC class II on (D) IECs in the ileum. (E) MHC class II MFI on IECs and splenic DCs (n = 4–5 per group from 2 replicate experiments).

(F and G) B6.WT and B6.*Il17ra*$^{-/-}$ mice were housed separately or cohoused for 6 weeks. (F) Representative histograms of MHC class II on IECs and (G) frequency of MHC class II$^+$ IECs (n = 8–10 per group combined from 2 replicate experiments).

(H) Cohoused or individually housed B6.WT mice were transplanted with CD4$^+$ T cells from BALB/c^{luc+} mice.

Quantification and representative images of day 7 bioluminescence (BLI) data (allogeneic CD4$^+$ T cell expansion) combined from 2 replicate experiments (n = 9–10 per group) are shown. Statistical analysis by unpaired t test (H), ANOVA (ileum and spleen in B and ileum in E and G), and Kruskal-Wallis test (spleen in E) (mean ± SEM). *p < 0.05, **p < 0.01, ***p < 0.001, ****p < 0.0001.

See also Figure S1.

carboxyfluorescein succinimidyl ester (CFSE)-labeled Marilyn T cells and examined Marilyn T cell activation and proliferation 7 days later by measuring CD69 expression and CFSE dilution, respectively. We found that male ileal MHC class II$^+$ IECs could stimulate Marilyn T cells (Figure 3A; Figures S2A and S2B). Ileal MHC class II$^+$ IECs did not express costimulatory molecules at steady state, but they did exhibit increased expression of CD80 after TBI (Figures S2C and S2D), and inhibition of CD80 in the cocultures with an anti-CD80 monoclonal antibody attenuated the stimulatory capacity of IECs after TBI (Figure S2E). Thus, IEC MHC class II expression can drive the proliferation of naive CD4$^+$ T cells.

We then focused on the molecular mechanisms controlling MHC class II expression in IECs at steady state, before and after BMT. We performed RNA sequencing (RNA-seq) analysis using sort-purified IECs (CD45^{neg} Villin-YFP$^+$) from the small intestine of naive mice, mice post-TBI, and mice post-BMT (after TBI and with grafts including T cells) (Figure 3B). Principal-component analysis (PCA) of gene expression profiles separated naive mice from the other two groups, indicating that

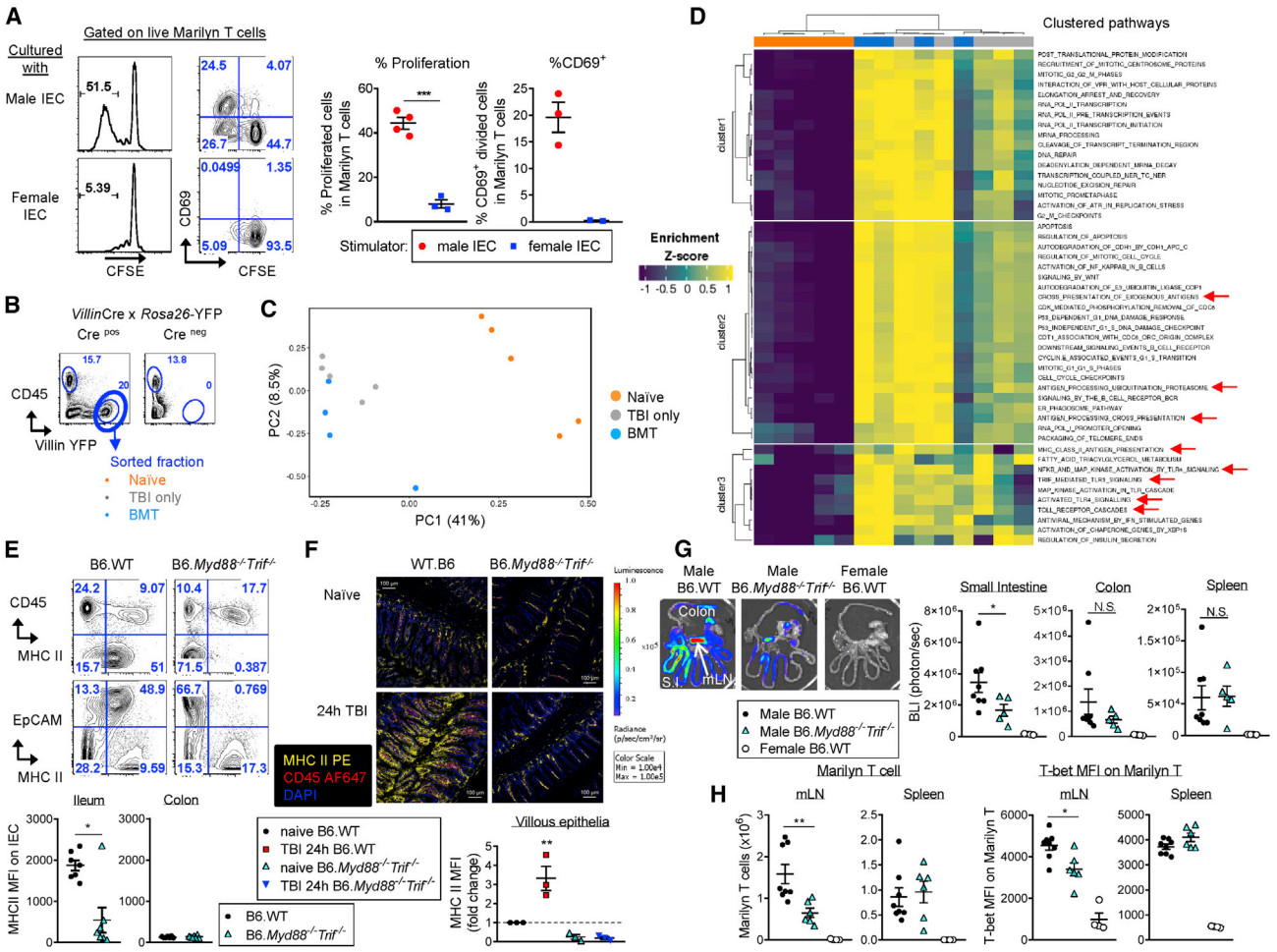

Figure 3. MyD88 and TRIF Signaling Are Necessary for MHC Class II Expression by IECs in the Ileum Pretransplant

(A) Mixed lymphocyte reaction (MLR) of CFSE-labeled, sort-purified, HY-reactive Marilyn CD4$^+$ T cells cocultured with sort-purified 7AAD^{neg}EpCAM$^+$CD45^{neg} IECs from the small intestine of irradiated male (HY-positive) or female (HY-negative) mice, analyzed at day 7. Data are representative of 3 replicate experiments (n = 3–4).

(B) Epithelial cells from the small intestine (7AAD^{neg}Villin$^+$CD45^{neg}) of naive *Villin*Cre^{pos}*Rosa26*-YFP mice. Those day 4 post-TBI or day 3 post-BMT were sort-purified and processed for RNA-seq gene expression analysis (n = 4–5 per group).

(C) First and second principal component projections.

(D) Clustered heatmap of the top 50 gene sets that significantly differentially increased at a false discovery rate (FDR) < 0.05 between groups of samples analyzed using ssGSEAs.

(E) Representative flow plots and MFI of MHC class II expression in the epithelial fractions from naive B6.WT and B6.*Myd88*$^{-/-}$*Trif*$^{-/-}$ mice. Data combined from 2 replicate experiments (n = 7 per group).

(F) Representative confocal images of MHC class II expression on ileum before and 24 h after TBI with quantification normalized to naive WT mice (n = 3 per group).

(G and H) Male B6.WT and B6.*Myd88*$^{-/-}$*Trif*$^{-/-}$ mice were transplanted with Marilyn^{luc+} T cells and analyzed on day 7. WT female recipients were used as negative controls (n = 4) and (n = 5–8 per male group combined from 2 replicate experiments).

(G) Representative BLI images and signal quantification in small intestine, colon, and spleen are shown.

(H) Marilyn^{luc+} T cell quantification and T-bet expression in mLNs and spleen.

Statistical analysis by unpaired t test (A), Mann-Whitney U test (E, G, and H), or ANOVA (F) (mean ± SEM). *p < 0.05, **p < 0.01, ***p < 0.001.

See also Figures S2–S4.

the transcriptional landscape of IECs is most influenced by TBI (Figure 3C). Single-sample gene set enrichment analyses (ssGSEAs) indicated that expression of genes associated with antigen presentation and processing pathways was augmented in both mice receiving TBI alone and those receiving T cell-replete grafts that developed GVHD (Figure 3D; Figures S2F and S3). These pathways appeared in three distinctive clusters. Cluster 1 included genes involved in the cell cycle and transcription. Multiple pathways related to antigen processing were tightly linked in cluster 2. Cluster 3 involved MHC class II antigen presentation pathways, together with Toll-like receptor (TLR)-driven signaling cascades, including multiple pathways downstream of TLR3 and TLR4 (Figure 3D; Figures S2F and S3).

Given the juxtaposition of IECs and the gut microbiota, and the importance of the latter to GVHD (Hayase et al., 2017; Jenq et al., 2012; Shono et al., 2016), we investigated the relationship between TLR signaling and MHC class II antigen presentation in the GI tract. We compared the ileum and colon from naive B6 (B6.WT) mice and from mice deficient for the TLR signaling adaptors MyD88 and TRIF (B6.*Myd88*$^{-/-}$*Trif*$^{-/-}$). MHC class II expression in hematopoietic populations (CD45^{+} EpCAM^{neg}) of B6.WT and B6.*Myd88*$^{-/-}$*Trif*$^{-/-}$ mice was comparable. However, IECs (CD45^{neg} EpCAM^{+}) from B6.*Myd88*$^{-/-}$*Trif*$^{-/-}$ mice lacked MHC class II expression both at steady state and after TBI (Figures 3E and 3F; Figure S4A). To determine the relevance of this pathway to donor T cell expansion, we transplanted luciferase-expressing Marilyn T cells into male B6.WT or B6.*Myd88*$^{-/-}$*Trif*$^{-/-}$ recipients and measured their proliferation. T cell expansion was reduced in the small intestine, but not in the colon or spleen, of B6.*Myd88*$^{-/-}$*Trif*$^{-/-}$ recipients (Figure 3G), consistent with the expression pattern of MHC class II on IECs. Furthermore, higher frequencies of Marilyn T cells were detected in the draining mesenteric lymph nodes (mLNs) of WT recipients compared with *Myd88*$^{-/-}$*Trif*$^{-/-}$ recipients, and these cells expressed the transcription factor T-bet, a hallmark of T helper 1 (Th1) differentiation (Figure 3H). To determine whether the requirement for TLR signaling in IEC MHC class II expression lays within the hematopoietic or the non-hematopoietic compartment, we used bone marrow (BM) chimeras in which hematopoietic cells, non-hematopoietic cells, or combinations thereof were deficient in Myd88 and TRIF. Expression of MyD88 and TRIF was required in both hematopoietic and non-hematopoietic compartments for the full induction of MHC class II expression on IECs (Figures S4B and S4C).

IFNγ Is Secreted by Recipient ILC1 and Conventional T Cells in the Small Intestine

We next examined the role of IFNγ in IEC MHC class II expression, because this cytokine is known to potently induce MHC class II expression in epithelial cells (Skoskiewicz et al., 1985). IECs from B6 WT mice expressed the IFNγ receptor (IFNγR) at steady state as measured by flow cytometry (Figure 4A), and B6.*Ifngr*$^{-/-}$ mice did not express MHC class II on IECs, either at steady-state or after TBI (Figures 4B and 4C; Figure S4A). To delineate the potential sources of IFNγ driving the expression of MHC class II, we analyzed MHC class II expression in the intestine of *Rag*$^{-/-}$*Il2rg*$^{-/-}$ mice, which lack innate and adaptive lymphocyte populations, and *Rag*$^{-/-}$ mice, which lack conventional TCR-rearranged T cells, pre- and post-TBI. MHC class II expression in the ileum was lost in *Rag*$^{-/-}$*Il2rg*$^{-/-}$ mice and decreased in *Rag*$^{-/-}$ mice (Figures 4D and 4E). Flow cytometric analysis of lamina propria lymphocytes from naive *Ifng*-YFP reporter mice demonstrated that among innate cell populations, IFNγ expression was predominantly in CD200r^{+} ILC1 (Weizman et al., 2017) (Figure 4F; Figures S5B and S5C). In naive mice, IFNγ expression was also observed in adaptive lymphocytes, primarily CD4^{+} T cells (Figure 4F). MHC class II expression in the ileum of *Rag*$^{-/-}$ mice did not increase after TBI (Figure 4E; Figure S5A). The TBI-induced IFNγ was predominantly observed in conventional T cells (CD4^{+} Tcon cells and CD8^{+} Tcon cells), and to a smaller extent in natural killer (NK) T cells, rather than innate lymphocyte populations, and was primarily seen in conventional T cells in the GI tract, but not in T cells in the draining mLNs (Figure 4G; Figure S5D). To determine whether the induction of MHC class II expression by IECs was a direct effect of IFNγ, we cultured intestinal organoids from the small intestine of B6.*I-A*^{b}β-GFP or B6.WT mice with or without IFNγ. EpCAM^{+} cells in organoids did not express MHC class II under standard culture conditions, but they did so rapidly in the presence of IFNγ (Figure 4H; Figure S5E). IFNγ also induced MHC class II expression (HLA-DR/DQ/DP) in human small intestine organoid cultures (Figure 4I). Altogether, these results suggest that MHC class II expression on IECs in the ileum can induce localized T cell activation and IFNγ secretion and that, in the context of GVHD, TBI induces a local cytokine feedforward cascade that amplifies MHC class II expression on IECs.

IECs Are Sufficient to Induce MHC Class II-Dependent GVHD

We next investigated whether MHC class II antigen presentation by IECs could initiate acute GVHD. We previously demonstrated that host non-hematopoietic APCs, including cells of mesenchymal origin, can also express MHC class II (Koyama et al., 2011). We therefore used three murine lines expressing Cre recombinase (Cre) driven off *Villin*, *Nestin*, and *Tie2* promoters, which are lineage markers for IECs, mesenchymal cells, and endothelial cells, respectively, to define the relevance of MHC class II expressed by these non-hematopoietic cell populations in the GI tract in driving GVHD. Lineage-restricted expression in the intestine was determined by Cre-driven YFP expression. Villin-expressing cells were EpCAM^{+}CD45^{neg} cells and aligned on the surface of villi. Nestin-expressing cells were CD45^{neg}Vimentin^{+} α-smooth muscle actin (αSMA)$^{+}$, consistent with mesenchymal cells. CD45^{neg} Tie2-expressing cells were CD31^{+}Ter119^{neg} endothelial cells (Figure 5A; Figure S6A). I-A^{b} is the MHC class II molecule expressed in B6 mice, and its expression can be deleted from Cre-expressing (Cre^{pos}) cell lineages using a floxed *I-A*^{b} gene (*I-A*$^{b\text{-}fl/fl}$) (Hashimoto et al., 2002). Next, we compared GVHD lethality between transplanted mice in which lineage-restricted non-hematopoietic cells can (Cre^{neg}) or cannot (Cre^{pos}) present MHC class II-loaded alloantigen. B6 male *Nestin*, *Villin*, or *Tie2* Cre^{pos}*I-A*$^{b\text{-}fl/fl}$ mice and relevant Cre^{neg}*I-A*$^{b\text{-}fl/fl}$ mice were reconstituted with female *I-A*^{b}-deficient bone marrow (B6.*I-A*$^{b-/-}$ BM), thus generating BM chimeras lacking the capacity for antigen presentation by hematopoietic APCs (Figures S6B–S6D). Three months later, these BM chimeras were used as BMT recipients and transplanted with female B6.*I-A*$^{b-/-}$ BM (to reconstitute hematopoiesis while preventing antigen presentation by donor APCs) and Marilyn T cells. GVHD mortality invoked by Marilyn T cells in response to alloantigen presented in recipient MHC class II was initiated by Villin-expressing cells, and less so by Nestin-expressing cells (Figure 5B). A significant reduction in luciferase-expressing Marilyn T cell expansion in the gut was also noted when recipient Villin-expressing cells alone could not present antigen (Figure 5C). Thus, MHC class II expression on IECs can initiate lethal GVHD immune responses.

MHC Class II-Expressing IECs Are Necessary for the Induction of CD4^{+} T Cell-Dependent GVHD within the GI Tract

We examined the role of Villin-expressing cells in lethal acute GVHD using a second experimental system in which recipients

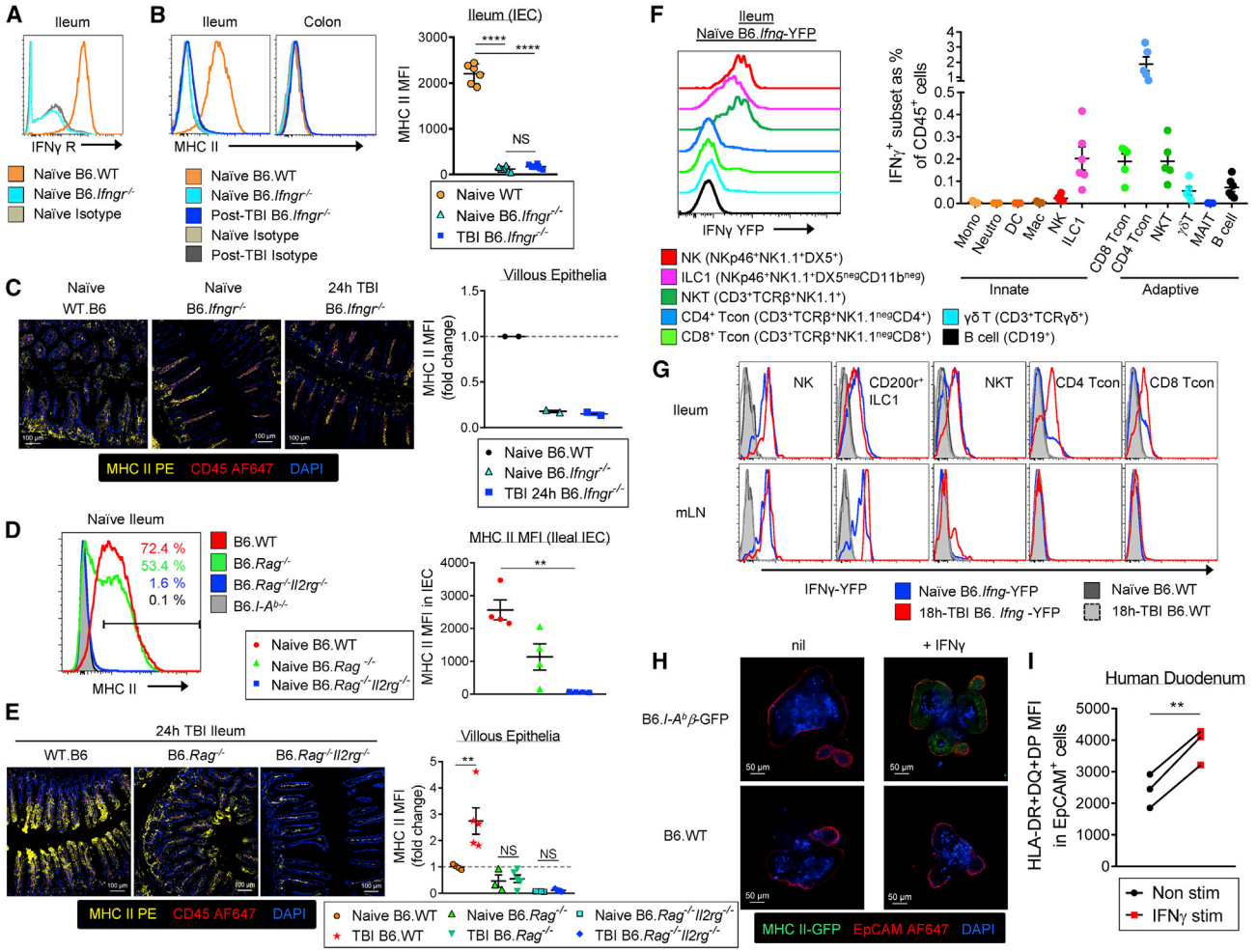

Figure 4. IFNγ Drives MHC Class II Expression on IECs

(A and B) Representative (A) IFNγR and (B) MHC class II expression on IECs (7AAD^{neg}EpCAM^{+}CD45^{neg}) from naive and 24 h post-TBI B6.WT and B6.*Ifngr*$^{-/-}$ mice. Quantified data (right) are combined from 3 replicate experiments (n = 6 per group).

(C) Fluorescence images of ileum from B6.*Ifngr*$^{-/-}$ (naive and 24 h post-TBI) and B6.WT (naive) mice. Representative images and quantification from 2 replicate experiments.

(D) Representative MHC class II expression on IECs from naive B6.WT, B6.*Rag*$^{-/-}$, B6.*Rag*$^{-/-}$*Il2rg*$^{-/-}$, and B6.*I-A*$^{b-/-}$ mice. Quantification is shown on the right (n = 4 per group from 3 experiments).

(E) Fluorescence images of ileum from 24 h post-TBI of B6.WT, B6.*Rag*$^{-/-}$, and B6.*Rag*$^{-/-}$*Il2rg*$^{-/-}$ mice. Representative images (left) and quantification from 2 replicate experiments are shown (n = 3–5 per group).

(F) Representative IFNγ-YFP expression (left) and quantified data (right) in hematopoietic cell subsets within the ileum from naive mice are shown (n = 3–6 per group from 3 replicate experiments).

(G) IFNγ-YFP expression shown in the indicated populations from the ileum and mLNs of naive mice and 18 h after TBI.

(H) Representative confocal images of small intestinal organoids generated from B6.*I-A*^{b}*β*-GFP or B6.WT mice in the presence or absence of IFNγ. Representative images from 2 replicate experiments.

(I) Flow cytometric quantification of HLA class II MFI in 7AAD^{neg}EpCAM^{+}CD45^{neg} cells from human duodenum organoids before and after IFNγ stimulation (healthy donors, n = 3, paired t test).

Multiple comparisons by ANOVA (B and E) or Kruskal-Wallis test (D) (mean ± SEM). *p < 0.05, **p < 0.01, ****p < 0.0001.

See also Figure S5.

express tamoxifen-dependent Cre recombinase under the control of the *Villin* promoter (*Villin*Cre-ER^{T2}) (Adolph et al., 2013; el Marjou et al., 2004). This allowed us to interrogate the role of IECs as APCs in a physiologically relevant manner, whereby donor and host hematopoietic APCs are intact but mice have (Cre-ER$^{T2\text{-}neg}$*I-A*$^{b\text{-}fl/fl}$) or lack (Cre-ER$^{T2\text{-}pos}$*I-A*$^{b\text{-}fl/fl}$) MHC class II specifically on IECs after tamoxifen administration (Figures S6E and S6F). Despite the presence of all other types of APCs, the lack of MHC class II^{+} IECs resulted in profound protection from acute GVHD lethality (Figure 6A). Consistent with this, these mice exhibited reduced levels of serum tumor necrosis factor (TNF) (Figure 6B) and decreased Marilyn T cell expansion in the gut and mLNs, but not other peripheral sites (Figures 6C and 6D; Figure S7A). In addition, a lower frequency of

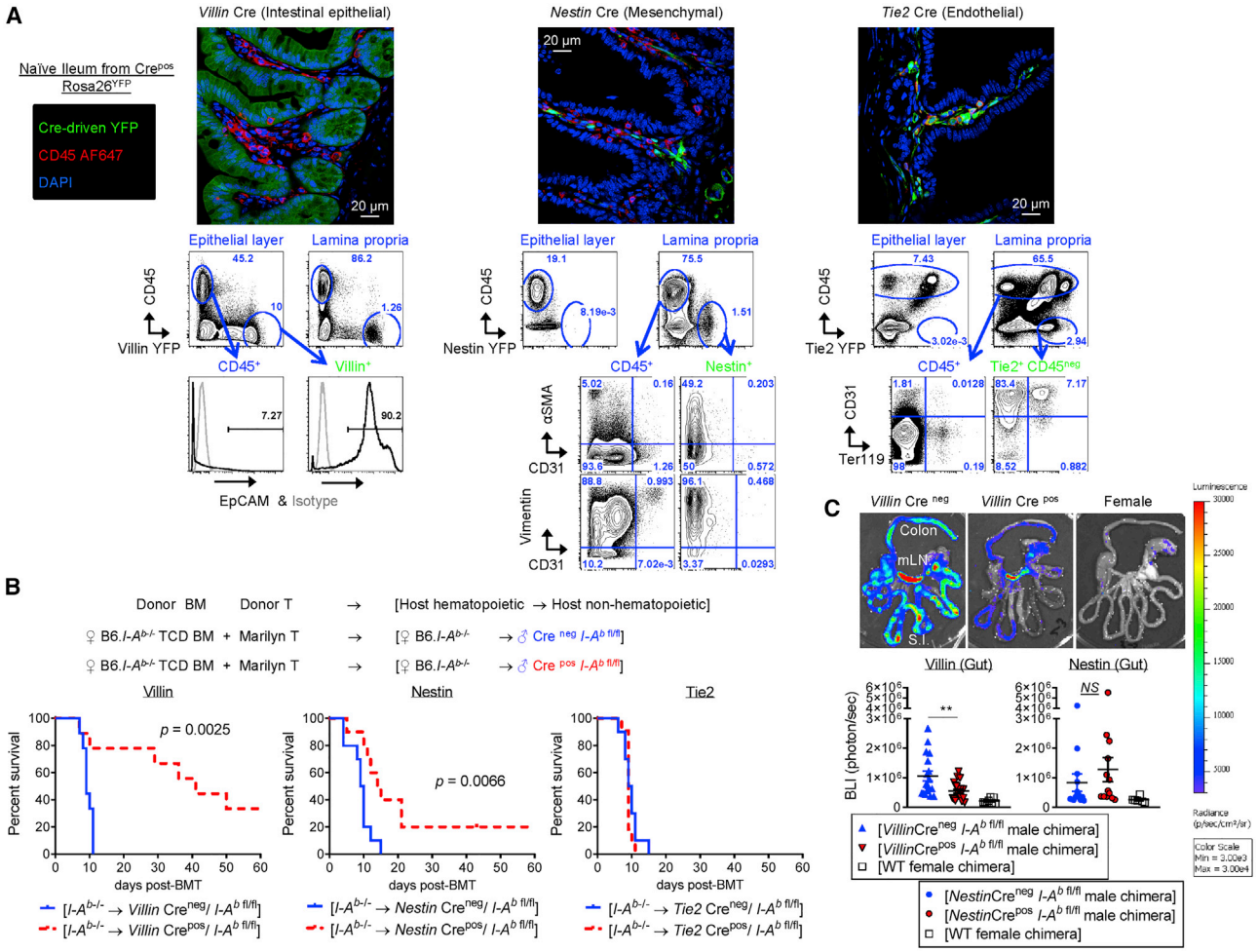

Figure 5. IECs Induce MHC Class II-Dependent GVHD

(A) Distribution (top: confocal images) and lineage (bottom: flow cytometry) of YFP$^+$ cells in the ileum from naive *Villin*Cre^{pos}*Rosa26*-YFP, *Nestin*Cre^{pos}*Rosa26*-YFP, or *Tie2*Cre^{pos}*Rosa26*-YFP mice. Representative of two replicate experiments.

(B) B6 male *Nestin*, *Villin*, or *Tie2* Cre^{pos}*I-A*$^{b\text{-}fl/fl}$ mice and relevant Cre^{neg}*I-A*$^{b\text{-}fl/fl}$ mice were transplanted with BM from female B6.*I-A*$^{b-/-}$ mice. Three months later, these chimeric mice were transplanted with BM from female B6.*I-A*$^{b-/-}$ mice and 25 × 10^3 sorted Marilyn T cells. Survival by Kaplan-Meier analysis, combined from 2 replicate experiments (n = 9–11 per group). p = 0.0025 (*Villin*), p = 0.0066 (*Nestin*): Cre^{pos}*I-A*$^{b\text{-}fl/fl}$ versus Cre^{neg}*I-A*$^{b\text{-}fl/fl}$ chimeric recipients.

(C) BM chimeric recipients were transplanted as in (B), but with 0.2 × 10^6 sorted Marilyn^{luc+} T cells. Representative BLI images and quantitative data on day 7 combined from 3–4 replicate experiments are shown (n = 12–21 per group).

Two-tailed unpaired t test (mean ± SEM); **p = 0.0090; N.S., not significant.

See also Figure S6.

Marilyn T cells recovered from the mLNs of these mice expressed T-bet (Figure 6E; Figure S7B), and GVHD pathology in the GI tract was ameliorated (Figures 6F and 6G). We corroborated these findings in an allogeneic system in which GVHD was mediated by polyclonal T cells. WT polyclonal CD4$^+$ T cells from BALB/c mice (H-2^d) were transplanted into MHC-mismatched female *Villin*Cre-ER$^{T2\text{-}neg}$*I-A*$^{b\text{-}fl/fl}$ or Cre-ER$^{T2\text{-}pos}$*I-A*$^{b\text{-}fl/fl}$ recipients (H-2^b). *Villin*Cre-ER$^{T2\text{-}pos}$*I-A*$^{b\text{-}fl/fl}$ recipients did not develop gut GVHD in this setting (Figures 6H–6J), although they did develop severe cutaneous GVHD that eventually required the mice to be euthanized (Figure 6K). Thus, in this scenario, polyclonal donor CD4$^+$ T cells could be primed and redirected by alternate APCs to other GVHD target organs (e.g., skin).

IL-12 Neutralization Prevents MHC Class II Expression by IEC Pretransplant and Averts CD4$^+$ T Cell-Dependent GVHD Lethality

Next, we examined the effects of pretransplant microbiota depletion on GVHD in the GI tract and the role of donor T cell-derived IFNγ on the expression of MHC class II by IECs after BMT. We transplanted male recipients, who had or had not received antibiotic-mediated microbiota decontamination, with Marilyn T cells. Three days after transplant, MHC class II expression on IECs remained low in microbiota-depleted recipients and was similar to non-GVHD controls (Figure 7A). In conjunction with this, T-bet expression remained low in recipient ILC1 (Figure 7B). Nevertheless, systemic IFNγ was produced in microbiota-depleted recipients receiving donor alloreactive T cells

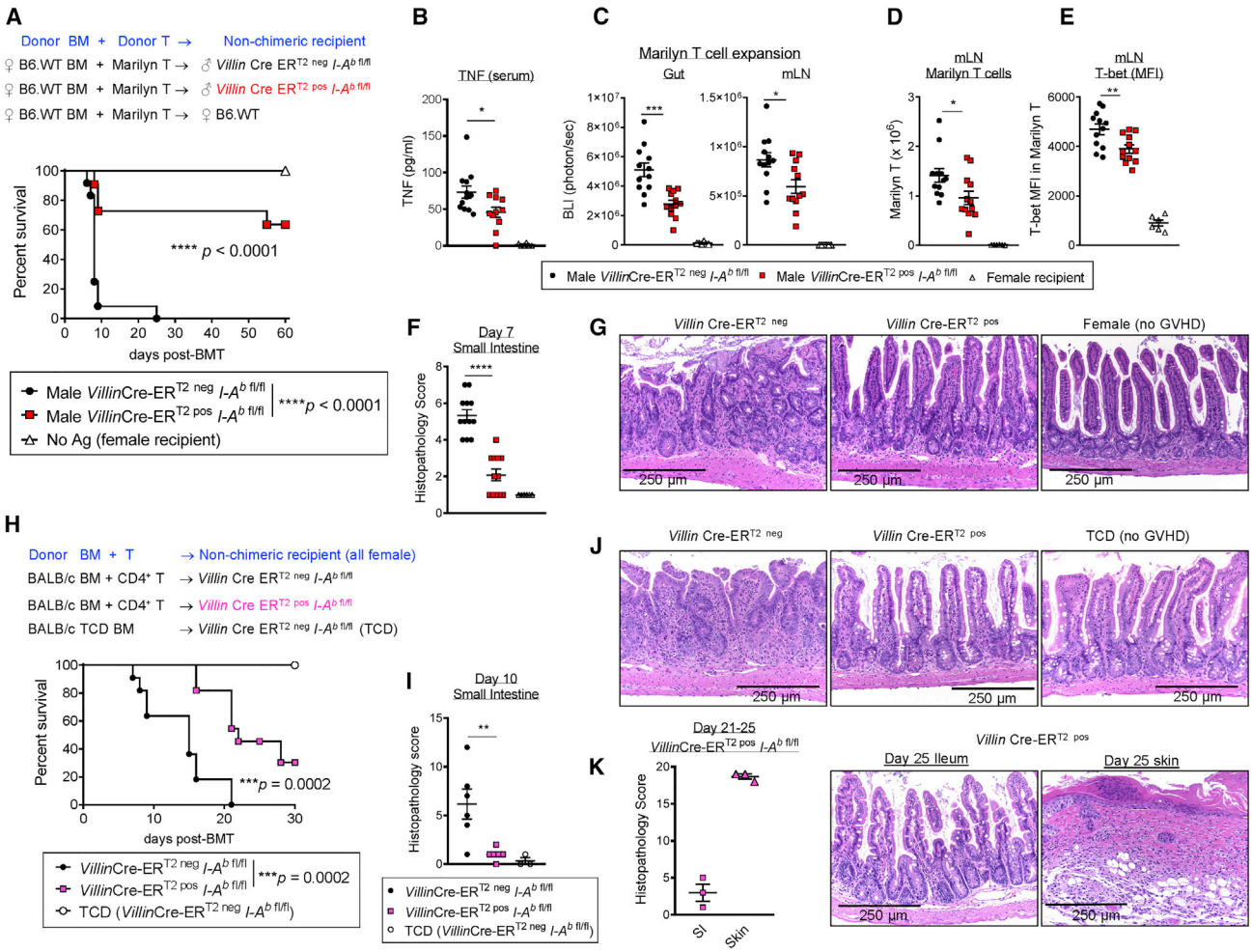

Figure 6. MHC Class II-Expressing IECs Elicit Alloantigen Reactive T Cell Expansion and Th1 Differentiation in the GI Tract

(A–K) Male (A–G) or female (H–K) *Villin* Cre-ER$^{T2\text{-}neg}$*I-A*$^{b\text{-}fl/fl}$ and Cre-ER$^{T2\text{-}pos}$*I-A*$^{b\text{-}fl/fl}$ mice or female B6.WT mice (A–G) were treated with tamoxifen 2 weeks before transplant.

(A) Tamoxifen-treated mice were transplanted with B6.WT BM with 0.5 × 10^6 CD4 magnetic-activated cell sorting (MACS)-purified Marilyn T cells. Female recipients are negative controls. Survival by Kaplan-Meier analysis, combined from 2 replicate experiments (n = 11–12 per T cell-replete group).

(B–G) Recipients were transplanted as in (A) but with 0.2 × 10^6 sorted Marilyn^{luc+} T cells. (B) Serum TNF, (C) BLI data, (D) enumeration of Marilyn T cells with (E) MFI of T-bet expression, and (F) intestinal histology with (G) representative images on day 7 are shown, combined from 3 replicate experiments (n = 12 per T cell-replete group).

(H–K) Lethally irradiated tamoxifen-treated female mice were transplanted with BM and regulatory T cell-depleted CD4$^+$ T cells from PC61-treated BALB/c mice.

(H) Survival by Kaplan-Meier analysis, combined from 2 replicate experiments (n = 11 per T cell-replete group).

(I and J) (I) Intestinal histopathology scores and (J) representative images on day 10 (n = 6 per T cell-replete group).

(K) Late skin and small intestine (SI) histology (n = 3).

*p < 0.05, **p < 0.01, ***p < 0.001, ****p < 0.0001: *Villin* Cre-ER$^{T2\text{-}neg}$*I-A*$^{b\text{-}fl/fl}$ versus Cre-ER$^{T2\text{-}pos}$*I-A*$^{b\text{-}fl/fl}$. Statistical analysis by two-tailed Mann-Whitney U test (B–F) or t test (I) (mean ± SEM), except for survival data.

See also Figures S6 and S7.

by day 3 after BMT, albeit at a lower level than recipients with an intact microbiota (Figure 7C). Consistent with this, MHC class II expression increased in these recipients by day 7 after transplant, although this did not reach the levels seen in animals in which the microbiota was intact (Figure 7D). Marilyn T cell infiltration in the gut of microbiota-depleted recipients was markedly attenuated, and acute GVHD histopathology was prevented (Figure 7D). We next explored the role of interleukin-12 (IL-12) in the IFNγ-dependent induction of MHC class II expression by IECs, because IFNγ responses are characteristically driven by IL-12 secretion from myeloid lineages (Biron and Tarrio, 2015). Flow cytometric analysis of B6.*IL-12/23p40*-YFP mice demonstrated that IL-12/23p40 was preferentially expressed by macrophages and, to a lesser extent, DCs in ileum lamina propria preparations (Figure 7E) and that IL-12 expression increased after TBI (Figure 7F). Antibiotic treatment reduced the number of IL-12/23p40-YFP$^+$ cells in the ileum of mice pretransplant (i.e., after TBI and before cell infusion) (Figures 7G and 7H). Mice

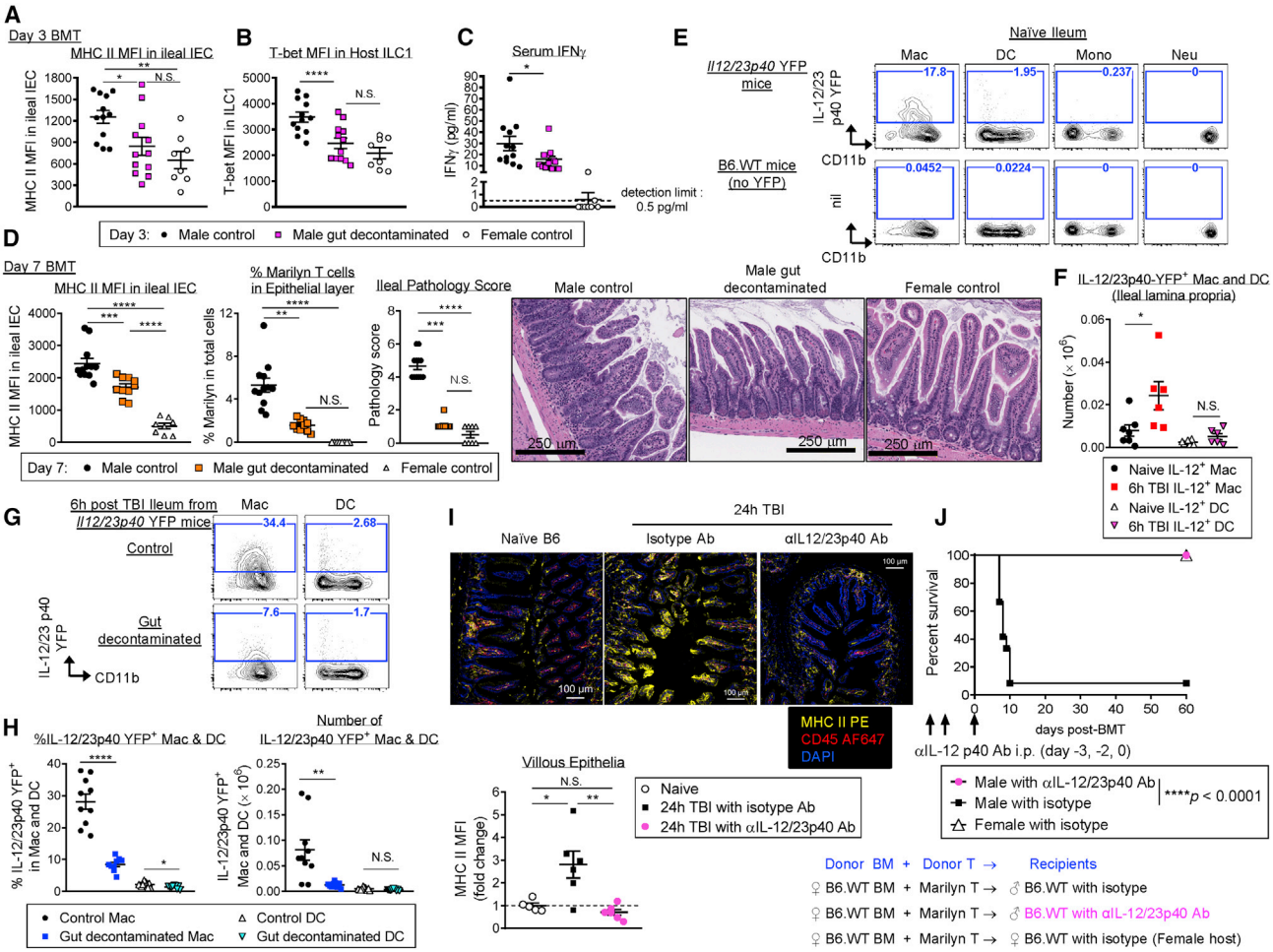

Figure 7. Neutralizing IL-12 before Irradiation Prevents the Induction of MHC Class II Expression on IEC Pretransplant and Subsequent GVHD

(A–D, G, and H) B6.WT mice (A–D) and B6.*Il12/23p40*-YFP mice (G and H) received either antibiotic water or normal water for 2 weeks.

(A–D) Lethally irradiated male B6.WT gut-decontaminated mice and control male and female mice were transplanted with 0.2 × 10^6 Marilyn T cells.

(A–C) Ileum was analyzed on day 3. (A) MHC class II expression quantified on IECs ($EpCAM^+CD45^{neg}$), (B) T-bet MFI in host ILC1, and (C) serum IFNγ (n = 8–12 per group from 2 replicate experiments, Mann-Whitney U test, C).

(D) Quantification of MHC class II expression on IECs (left), frequency of Marilyn T cells infiltrating the epithelial fraction (middle), and ileum GVHD histopathology scores (right), with representative H&E-stained images on day 7, are shown (n = 8–12 per group from 2 replicate experiments).

(E) Representative flow plots of IL-12/23p40-YFP expression on macrophages (Mac), DCs, monocytes (Mono), and neutrophil (Neu) from naive B6.*Il12/23p40*-YFP mice (from 3 replicate experiments). B6.WT mice were gated as negative controls.

(F) Quantification of *Il12/23p40*-YFP^+ Mac and DCs from naive mice or 6 h post-TBI (n = 6–7 per group from 3 replicate experiments, unpaired t test).

(G and H) Representative flow plots (G) and frequency (left) and numbers (right) of IL-12/23p40-YFP^+ cells (H) in the ileum of mice 24 h after TBI (n = 9–10 per group from 2 replicate experiments, unpaired t test).

(I) B6.WT mice were treated with IL-12/23p40 monoclonal antibody (mAb) or isotype control 48 and 24 h before TBI. Representative ileal images are shown with quantification (n = 5–6 per group from 2 replicate experiments).

(J) Survival by Kaplan-Meier estimates. Male B6.WT mice were treated with IL-12/23p40 mAb or isotype control at 48 h (day -3) and 24 h (day -2) before TBI and day 0, before the infusion of B6.WT BM and Marilyn T cells (n = 12 combined from 2 replicate experiments). Female recipients (n = 4) were used as negative controls.

Multiple comparisons by ANOVA, except (D) (ileal pathology) and Kruskal-Wallis test (mean ± SEM). *p < 0.05, **p < 0.01, ****p < 0.0001.

See also Figure S7.

treated with anti-IL-12/23p40 before TBI did not exhibit increased MHC class II expression by IEC pretransplant (Figure 7I; Figure S7C), and this treatment decreased acute GVHD lethality (Figure 7J). Finally, the expression of MHC class II by IECs in the ileum pretransplant was abrogated in *Il12p35*$^{-/-}$ recipients, pointing to a critical role for IL-12 in IEC MHC class II expression (Figure S7D).

DISCUSSION

Gut pathology is a key initiator of GVHD after allogeneic BMT. Characterization of the cellular and molecular mechanisms that initiate gut disease is key to identifying pathways that can be targeted therapeutically. Here we established a pivotal role for IECs in MHC class II-dependent antigen presentation and thereby in

the initiation of GVHD in the GI tract. We also showed that the microbiota controlled MHC class II expression by IECs both at steady-state and during inflammation induced by conditioning. This required an IL-12/IFNγ cytokine axis that could be targeted therapeutically to block $CD4^+$ T cell-dependent GVHD.

The interactions between microbiota and host immunity are well defined and involve various Danger-associated molecular oattern (DAMP)/pathogen-associated molecular pattern (PAMP) signaling motifs, including TLRs, Nod-like receptors, and short-chain fatty acids (Chang et al., 2014; Vatanen et al., 2016). However, the ability of the microbiota to shape antigen presentation by gut epithelial cells has not been defined. Although MHC gene expression in the GI tract is linked to the microbiota (El Aidy et al., 2012), the cell subsets involved and subsequent responses have not been delineated. MHC class II expression on IECs, most highly in intestinal stem cells, controls epithelial-cell remodeling following infection (Biton et al., 2018); however, whether this MHC class II expression has a pathogenic role in the induction of disease is unknown. Here, we showed that (1) under homeostatic conditions, IL-12 secretion from macrophages induced IFNγ secretion by lamina propria lymphocytes in a microbiota and MyD88/TRIF-dependent manner, resulting in MHC class II expression by IECs in the ileum, and (2) MHC class II-expressing IECs functioned as APCs to prime donor $CD4^+$ T cells *in vivo* and induced lethal acute GVHD. Furthermore, conditioning with TBI invoked additional IL-12 secretion by macrophages in a microbiota-dependent manner and rapid IFNγ secretion by conventional T cells in the GI tract, which resulted in rapid and marked enhancement of MHC class II expression, together with CD80 expression by IECs. Critically, deletion of MHC class II in Villin-expressing enterocytes prevented disease by restraining donor $CD4^+$ T cell priming, differentiation, and GVHD in the GI tract. Reduced T-bet expression in T cells in the mLNs was noted, and we speculate that these cells migrate from the small intestine after priming, as previously described (Beura et al., 2018). Thus, we describe interactions between the microbiome and the immune cells in the GI tract pretransplant and show that when this balance is perturbed by inflammatory signals during conditioning, overt immunopathology ensues.

Our results have identified an axis of antigen presentation that drives disease in the GI tract after BMT and have defined pathways for therapeutic intervention that can be immediately tested. Although it is clear that hematopoietic cells include the principal APCs that drive MHC class I-dependent acute GVHD (Shlomchik et al., 1999; Toubai et al., 2012), this does not hold true for MHC class II-dependent acute GVHD (Koyama et al., 2011). Acute GVHD can be mediated by MHC class II-expressing hematopoietic cells (Teshima et al., 2002), but there has been no direct comparison with MHC class II-expressing non-hematopoietic cells, which appear dominant (Koyama et al., 2011). Here we demonstrated that the initiation phase of MHC class II-dependent acute GVHD required a cognate $CD4^+$ T cell-MHC class II interaction at the intestinal epithelial surface. We also showed that MyD88/TRIF pathways in both the hematopoietic and the non-hematopoietic compartment were involved, consistent with inhibition of these pathways in the hematopoietic compartment being insufficient to block MHC class II antigen presentation in the GI tract and subsequent GVHD (Li et al., 2011). Although non-hematopoietic cells may also respond to microbiota-derived signals to induce MHC class II expression on IECs and should be the subject of further study, in our studies the inhibition of microbiota-driven IL-12 pretransplant was sufficient to attenuate MHC class II expression by IECs and prevent acute GVHD lethality. Thus, we have identified IECs as the non-hematopoietic APCs involved in antigen presentation, thereby explaining the inability of approaches that delete hematopoietic professional recipient APCs to prevent acute GVHD in preclinical systems (Hashimoto et al., 2011; Koyama et al., 2011; Li et al., 2012; MacDonald et al., 2010; Rowe et al., 2006). Many professional APC subsets (e.g., DCs) do potently present alloantigen, but the net effect of this function is activation-induced cell death and/or phagocytosis (e.g., by macrophages) of donor $CD4^+$ T cells, which paradoxically attenuates GVHD (Hashimoto et al., 2011; Koyama et al., 2011; Markey et al., 2018). Thus, approaches to delete recipient DCs, macrophages, or even B cells are generally deleterious and instead amplify GVHD. In contrast, IECs presented endogenous alloantigen in a truly pathogenic fashion (because deletion attenuated GVHD), and this process was under strict control by soluble mediators secreted by hematopoietic APCs (i.e., IL-12) and lymphocytes (i.e., IFNγ) induced in response to the microbiota pretransplant. Although the mechanisms whereby the microbiome plays an important role in disease penetrance and phenotypes, including GVHD, are not understood (Jenq et al., 2012; Shono et al., 2016), it is clear that the transfer of dysbiotic GI tract microbiota can alter GVHD phenotypes (Varelias et al., 2017). The current data suggest that the control of antigen presentation within IECs is an important component of this interactive network that should be explored in other inflammatory diseases of the GI tract, particularly Crohn's disease, in which the terminal ileum is selectively involved. Finally, the role of DAMPs in this process is unclear and deserves further study.

The secretion of IFNγ by conventional recipient T cells within 24 h of TBI, in the absence of transplantation, was unexpected. Because this did not occur in secondary lymphoid organs despite significant IL-12 secretion at those sites, it seems that localized, likely tissue-resident, memory T cells respond to local TCR-dependent signals in the context of IL-12. It is likely that this reflects a response to local pathogen-derived peptide-MHC complexes that are absent from tissue-draining lymph nodes and drives a tissue-specific feedforward cascade in the GI tract. Systemic neutralization of IL-12, commencing before TBI, prevented the increase of IFNγ-dependent expression of MHC class II by IECs that initiated acute GVHD. This finding is consistent with exogenous IL-12 administration after TBI exacerbating gut GVHD (Hixon et al., 2002). Several lines of evidence suggest that IFNγ acts directly on IECs to invoke antigen presentation. First, the addition of exogenous IFNγ to organoids that do not contain hematopoietic cells induced MHC class II expression. Second, the ability of IFNγ to induce intestinal GVHD requires expression of IFNγR on parenchymal cells only (Burman et al., 2007). IFNγ from donor $CD4^+$ T cells may damage MHC class II-expressing IECs indirectly, without cognate MHC-TCR interaction, as previously described (Teshima et al., 2002), and this deserves further study. The inhibition of IFNγ after BMT results in severe acute lung injury (Burman et al., 2007; Varelias et al., 2015); thus, this approach is not feasible in the clinic. IFNγ can

be generated by alloreactive donor T cells in response to APCs that are not IECs, and this can in turn augment MHC class II expression by IECs. IECs in antibiotic-treated mice expressed MHC class II post-transplant (i.e., beyond day 3), yet there was no significant T cell expansion or gut GVHD by histopathology relative to non-GVHD controls, which is consistent with the notion that the early expression of MHC class II (before day 3) on IECs is critical in initiating gut GVHD.

Nevertheless, generation of IFNγ by alloreactive T cells has the potential to invoke a feedforward loop of antigen presentation by IECs after transplant. That said, this phenomena is likely to be less relevant in clinical transplantation, in which T cell-dependent effector cytokine responses, including IFNγ, are prevented by standard immune suppression with calcineurin inhibitors and methotrexate early after BMT (Kennedy et al., 2014).

Our results demonstrated that the microbiota controls MHC class II on IEC pretransplant (including after TBI but before cell infusion) and that this pathway can contribute to the initiation of GVHD. However, this does not exclude additional effects of the microbiota after transplant that may be independent of MHC class II expression by IECs. These include the activation of other APCs and T cells that will contribute to the kinetics of GVHD, and these pathways should continue to be investigated. Given the successful therapeutic application of IL-12 inhibition to treat Crohn's disease (Feagan et al., 2016) and promising early results in BMT targeting T cell differentiation after transplant (Pidala et al., 2018), IL-12 inhibition starting before conditioning would appear to be an attractive adjunct approach to prevent GVHD. Our data also suggest that strategies to prevent GVHD based on host T cell depletion would be most efficacious when completed before the initiation of conditioning. Pretransplant inhibition with clinical IL-12 blocking antibodies that have a half-life of many weeks (Pidala et al., 2018) may also minimize the aforementioned feedforward loop of antigen presentation by IECs in response to donor T cell-derived IFNγ after BMT.

The crucial role for antigen presentation by IECs in the ileum as a distinct anatomical site is intriguing, particularly given that the colon is the site at which most microbiota-derived PAMP signals reside. Despite this, colon epithelial cells did not express high levels of MHC class II even after BMT, likely reflective of effective barrier function, including the extensive mucous layer present at this site, as opposed to the ileum. Studies confirm that the ileum is the anatomically weakest barrier site in the GI tract (Hülsdünker et al., 2018).

Although MHC class II expression by non-hematopoietic cells such as fibroblasts, endothelial cells, and epithelial cells has been described (Londei et al., 1984; Saada et al., 2006; Stevanovic et al., 2013), its functional role in antigen presentation has remained ambiguous. It has been considered to promote tolerance rather than inflammation (Kambayashi and Laufer, 2014; Thelemann et al., 2014). In relation to gut epithelia, HLA class II is expressed in the colon during GVHD or in infectious colitis after renal transplant (Stevanovic et al., 2013). Furthermore, colonic epithelial cells express HLA-DR in non-transplant patients with inflammatory bowel disease (IBD) and infectious colitis, whereas this is not the case in healthy donors (McDonald and Jewell, 1987). In addition, because the role of MHC class II is classically defined by exogenous antigen presentation following phagocytosis or endocytosis, the relative importance for endogenous antigen presentation, including alloantigen presentation, by MHC class II is less clear (Paludan et al., 2005; Roche and Furuta, 2015). Our results demonstrated that IECs presented alloantigen to $CD4^+$ T cells and could initiate GVHD, a finding with major implications for the pathogenesis of other inflammatory conditions involving the GI tract. Furthermore, our data highlighted several critical pathways that can be modulated before transplant to prevent the initiation of acute GVHD in the GI tract, focusing on the microbiota, PAMP signaling, and the downstream cytokines IL-12 and IFNγ.

STAR★METHODS

Detailed methods are provided in the online version of this paper and include the following:

- KEY RESOURCES TABLE
- LEAD CONTACT AND MATERIALS AVAILABILITY
- EXPERIMENTAL MODEL AND SUBJECT DETAILS
  - Mice
  - Stem Cell Transplantation
- METHOD DETAILS
  - Cell isolation from small intestine and colon
  - Gut decontamination
  - Mouse and human organoid isolation and growth protocol
  - Flow cytometry
  - Histologic analysis
  - Immunofluorescence microscopy
  - Mixed lymphocyte reaction (MLR)
  - Cytokine analysis
  - Bioluminescence imaging (BLI)
  - RNA sequencing
- QUANTIFICATION AND STATISTICAL ANALYSIS
- DATA AND CODE AVAILABILITY

SUPPLEMENTAL INFORMATION

Supplemental Information can be found online at https://doi.org/10.1016/j.immuni.2019.08.011.

ACKNOWLEDGMENTS

From QIMR Berghofer, we thank C. Winterford for expert preparation of histology samples; M. Rist, P. Hall, and G. Chojnowski for expert cell sorting; M. Flynn for expert generation of the graphics; and the animal facility for attentive animal care. We thank S. Robine (Institut Curie-CNRS, France) and R.S. Blumberg (Harvard Medical School, USA) for the *Villin*Cre-ER^{T2} mice. This work was supported by research grants from the National Health and Medical Research Council (NHMRC), Australia (APP1086685) and the National Heart, Lung, and Blood Institute of the NIH (R01HL148164), United States. The content is solely the responsibility of the authors and does not necessarily represent the official views of the NIH. M.K. was a Leukaemia Foundation of Australia fellow. N.W. is a NHMRC senior research fellow. M.A.D.-E. is a NHMRC principal research fellow. G.R.H. was a NHMRC senior principal research fellow. R.Z. is a fellow of Deutsche Krebshilfe (111639), Germany. B.R.B. is supported in part by the NIH (R37 AI34495).

AUTHOR CONTRIBUTIONS

M.K. designed, performed, and analyzed most experiments and wrote the paper. P.M. performed the bioinformatics analysis. I.S.S., A.V., and P.Z. helped design experiments. I.S.S., A.S.H., J.H., M.V., R.D.K., and R.J.R. performed

research. J.H. and A.D.C. performed the histological analysis. B.R.B., R.T., J.B., N.W., G.T., R.Z., and A.D.C. provided data interpretation. M.A.D.-E. helped design experiments and wrote the paper. G.R.H. designed experiments and wrote the paper. Results were discussed and the manuscript was critically commented on and edited by all authors.

DECLARATION OF INTERESTS

The authors declare no competing interests.

Received: November 29, 2018
Revised: May 15, 2019
Accepted: August 13, 2019
Published: September 18, 2019

REFERENCES

Adolph, T.E., Tomczak, M.F., Niederreiter, L., Ko, H.J., Böck, J., Martinez-Naves, E., Glickman, J.N., Tschurtschenthaler, M., Hartwig, J., Hosomi, S., et al. (2013). Paneth cells as a site of origin for intestinal inflammation. Nature *503*, 272–276.

Andermann, T.M., Peled, J.U., Ho, C., Reddy, P., Riches, M., Storb, R., Teshima, T., van den Brink, M.R.M., Alousi, A., Balderman, S., et al.; Blood and Marrow Transplant Clinical Trials Network (2018). The Microbiome and Hematopoietic Cell Transplantation: Past, Present, and Future. Biol. Blood Marrow Transplant. *24*, 1322–1340.

Beelen, D.W., Elmaagacli, A., Müller, K.D., Hirche, H., and Schaefer, U.W. (1999). Influence of intestinal bacterial decontamination using metronidazole and ciprofloxacin or ciprofloxacin alone on the development of acute graft-versus-host disease after marrow transplantation in patients with hematologic malignancies: final results and long-term follow-up of an open-label prospective randomized trial. Blood *93*, 3267–3275.

Beilhack, A., Schulz, S., Baker, J., Beilhack, G.F., Wieland, C.B., Herman, E.I., Baker, E.M., Cao, Y.A., Contag, C.H., and Negrin, R.S. (2005). *In vivo* analyses of early events in acute graft-versus-host disease reveal sequential infiltration of T-cell subsets. Blood *106*, 1113–1122.

Beura, L.K., Wijeyesinghe, S., Thompson, E.A., Macchietto, M.G., Rosato, P.C., Pierson, M.J., Schenkel, J.M., Mitchell, J.S., Vezys, V., Fife, B.T., et al. (2018). T Cells in Nonlymphoid Tissues Give Rise to Lymph-Node-Resident Memory T Cells. Immunity *48*, 327–338.e5.

Biron, C.A., and Tarrio, M.L. (2015). Immunoregulatory cytokine networks: 60 years of learning from murine cytomegalovirus. Med. Microbiol. Immunol. (Berl.) *204*, 345–354.

Biton, M., Haber, A.L., Rogel, N., Burgin, G., Beyaz, S., Schnell, A., Ashenberg, O., Su, C.W., Smillie, C., Shekhar, K., et al. (2018). T Helper Cell Cytokines Modulate Intestinal Stem Cell Renewal and Differentiation. Cell *175*, 1307–1320.e22.

Boes, M., Cerny, J., Massol, R., Op den Brouw, M., Kirchhausen, T., Chen, J., and Ploegh, H.L. (2002). T-cell engagement of dendritic cells rapidly rearranges MHC class II transport. Nature *418*, 983–988.

Burman, A.C., Banovic, T., Kuns, R.D., Clouston, A.D., Stanley, A.C., Morris, E.S., Rowe, V., Bofinger, H., Skoczylas, R., Raffelt, N., et al. (2007). IFNgamma differentially controls the development of idiopathic pneumonia syndrome and GVHD of the gastrointestinal tract. Blood *110*, 1064–1072.

Chang, P.V., Hao, L., Offermanns, S., and Medzhitov, R. (2014). The microbial metabolite butyrate regulates intestinal macrophage function via histone deacetylase inhibition. Proc. Natl. Acad. Sci. USA *111*, 2247–2252.

Cooke, K.R., Kobzik, L., Martin, T.R., Brewer, J., Delmonte, J., Jr., Crawford, J.M., and Ferrara, J.L.M. (1996). An experimental model of idiopathic pneumonia syndrome after bone marrow transplantation: I. The roles of minor H antigens and endotoxin. Blood *88*, 3230–3239.

Dobin, A., Davis, C.A., Schlesinger, F., Drenkow, J., Zaleski, C., Jha, S., Batut, P., Chaisson, M., and Gingeras, T.R. (2013). STAR: ultrafast universal RNA-seq aligner. Bioinformatics *29*, 15–21.

El Aidy, S., van Baarlen, P., Derrien, M., Lindenbergh-Kortleve, D.J., Hooiveld, G., Levenez, F., Doré, J., Dekker, J., Samsom, J.N., Nieuwenhuis, E.E., and Kleerebezem, M. (2012). Temporal and spatial interplay of microbiota and intestinal mucosa drive establishment of immune homeostasis in conventionalized mice. Mucosal Immunol. *5*, 567–579.

el Marjou, F., Janssen, K.P., Chang, B.H., Li, M., Hindie, V., Chan, L., Louvard, D., Chambon, P., Metzger, D., and Robine, S. (2004). Tissue-specific and inducible Cre-mediated recombination in the gut epithelium. Genesis *39*, 186–193.

Feagan, B.G., Sandborn, W.J., Gasink, C., Jacobstein, D., Lang, Y., Friedman, J.R., Blank, M.A., Johanns, J., Gao, L.L., Miao, Y., et al.; UNITI–IM-UNITI Study Group (2016). Ustekinumab as Induction and Maintenance Therapy for Crohn's Disease. N. Engl. J. Med. *375*, 1946–1960.

Ferrara, J.L., Levine, J.E., Reddy, P., and Holler, E. (2009). Graft-versus-host disease. Lancet *373*, 1550–1561.

Grusby, M.J., Johnson, R.S., Papaioannou, V.E., and Glimcher, L.H. (1991). Depletion of CD4+ T cells in major histocompatibility complex class II-deficient mice. Science *253*, 1417–1420.

Hashimoto, D., Chow, A., Greter, M., Saenger, Y., Kwan, W.H., Leboeuf, M., Ginhoux, F., Ochando, J.C., Kunisaki, Y., van Rooijen, N., et al. (2011). Pretransplant CSF-1 therapy expands recipient macrophages and ameliorates GVHD after allogeneic hematopoietic cell transplantation. J. Exp. Med. *208*, 1069–1082.

Hashimoto, K., Joshi, S.K., and Koni, P.A. (2002). A conditional null allele of the major histocompatibility IA-beta chain gene. Genesis *32*, 152–153.

Hayase, E., Hashimoto, D., Nakamura, K., Noizat, C., Ogasawara, R., Takahashi, S., Ohigashi, H., Yokoi, Y., Sugimoto, R., Matsuoka, S., et al. (2017). R-Spondin1 expands Paneth cells and prevents dysbiosis induced by graft-versus-host disease. J. Exp. Med. *214*, 3507–3518.

Hill, G.R., and Ferrara, J.L.M. (2000). The primacy of the gastrointestinal tract as a target organ of acute graft-versus-host disease: rationale for the use of cytokine shields in allogeneic bone marrow transplantation. Blood *95*, 2754–2759.

Hirota, K., Duarte, J.H., Veldhoen, M., Hornsby, E., Li, Y., Cua, D.J., Ahlfors, H., Wilhelm, C., Tolaini, M., Menzel, U., et al. (2011). Fate mapping of IL-17-producing T cells in inflammatory responses. Nat. Immunol. *12*, 255–263.

Hixon, J.A., Anver, M.R., Blazar, B.R., Panoskaltsis-Mortari, A., Wiltrout, R.H., and Murphy, W.J. (2002). Administration of either anti-CD40 or interleukin-12 following lethal total body irradiation induces acute lethal toxicity affecting the gut. Biol. Blood Marrow Transplant. *8*, 316–325.

Hülsdünker, J., Ottmüller, K.J., Neeff, H.P., Koyama, M., Gao, Z., Thomas, O.S., Follo, M., Al-Ahmad, A., Prinz, G., Duquesne, S., et al. (2018). Neutrophils provide cellular communication between ileum and mesenteric lymph nodes at graft-versus-host disease onset. Blood *131*, 1858–1869.

Jenq, R.R., Ubeda, C., Taur, Y., Menezes, C.C., Khanin, R., Dudakov, J.A., Liu, C., West, M.L., Singer, N.V., Equinda, M.J., et al. (2012). Regulation of intestinal inflammation by microbiota following allogeneic bone marrow transplantation. J. Exp. Med. *209*, 903–911.

Johansson, M.E., Phillipson, M., Petersson, J., Velcich, A., Holm, L., and Hansson, G.C. (2008). The inner of the two Muc2 mucin-dependent mucus layers in colon is devoid of bacteria. Proc. Natl. Acad. Sci. USA *105*, 15064–15069.

Kambayashi, T., and Laufer, T.M. (2014). Atypical MHC class II-expressing antigen-presenting cells: can anything replace a dendritic cell? Nat. Rev. Immunol. *14*, 719–730.

Kennedy, G.A., Varelias, A., Vuckovic, S., Le Texier, L., Gartlan, K.H., Zhang, P., Thomas, G., Anderson, L., Boyle, G., Cloonan, N., et al. (2014). Addition of interleukin-6 inhibition with tocilizumab to standard graft-versus-host disease prophylaxis after allogeneic stem-cell transplantation: a phase 1/2 trial. Lancet Oncol. *15*, 1451–1459.

Koyama, M., Cheong, M., Markey, K.A., Gartlan, K.H., Kuns, R.D., Locke, K.R., Lineburg, K.E., Teal, B.E., Leveque-El Mouttie, L., Bunting, M.D., et al. (2015). Donor colonic CD103+ dendritic cells determine the severity of acute graft-versus-host disease. J. Exp. Med. *212*, 1303–1321.

Koyama, M., and Hill, G.R. (2016). Alloantigen presentation and graft-versus-host disease: fuel for the fire. Blood *127*, 2963–2970.

Koyama, M., Kuns, R.D., Olver, S.D., Raffelt, N.C., Wilson, Y.A., Don, A.L., Lineburg, K.E., Cheong, M., Robb, R.J., Markey, K.A., et al. (2011).

Recipient nonhematopoietic antigen-presenting cells are sufficient to induce lethal acute graft-versus-host disease. Nat. Med. *18*, 135–142.

Lantz, O., Grandjean, I., Matzinger, P., and Di Santo, J.P. (2000). Gamma chain required for naïve CD4+ T cell survival but not for antigen proliferation. Nat. Immunol. *1*, 54–58.

Li, H., Demetris, A.J., McNiff, J., Matte-Martone, C., Tan, H.S., Rothstein, D.M., Lakkis, F.G., and Shlomchik, W.D. (2012). Profound depletion of host conventional dendritic cells, plasmacytoid dendritic cells, and B cells does not prevent graft-versus-host disease induction. J. Immunol. *188*, 3804–3811.

Li, H., Matte-Martone, C., Tan, H.S., Venkatesan, S., McNiff, J., Demetris, A.J., Jain, D., Lakkis, F., Rothstein, D., and Shlomchik, W.D. (2011). Graft-versus-host disease is independent of innate signaling pathways triggered by pathogens in host hematopoietic cells. J. Immunol. *186*, 230–241.

Londei, M., Lamb, J.R., Bottazzo, G.F., and Feldmann, M. (1984). Epithelial cells expressing aberrant MHC class II determinants can present antigen to cloned human T cells. Nature *312*, 639–641.

MacDonald, K.P., Palmer, J.S., Cronau, S., Seppanen, E., Olver, S., Raffelt, N.C., Kuns, R., Pettit, A.R., Clouston, A., Wainwright, B., et al. (2010). An antibody against the colony-stimulating factor 1 receptor depletes the resident subset of monocytes and tissue- and tumor-associated macrophages but does not inhibit inflammation. Blood *116*, 3955–3963.

Markey, K.A., Kuns, R.D., Browne, D.J., Gartlan, K.H., Robb, R.J., Martins, J.P., Henden, A.S., Minnie, S.A., Cheong, M., Koyama, M., et al. (2018). Flt-3L Expansion of Recipient CD8α^+ Dendritic Cells Deletes Alloreactive Donor T Cells and Represents an Alternative to Posttransplant Cyclophosphamide for the Prevention of GVHD. Clin. Cancer Res. *24*, 1604–1616.

Martin, M. (2011). Cutadapt Removes Adapter Sequences From High-Throughput Sequencing Reads. EMBnet *17*.

Mathewson, N.D., Jenq, R., Mathew, A.V., Koenigsknecht, M., Hanash, A., Toubai, T., Oravecz-Wilson, K., Wu, S.R., Sun, Y., Rossi, C., et al. (2016). Gut microbiome-derived metabolites modulate intestinal epithelial cell damage and mitigate graft-versus-host disease. Nat. Immunol. *17*, 505–513.

McDonald, G.B., and Jewell, D.P. (1987). Class II antigen (HLA-DR) expression by intestinal epithelial cells in inflammatory diseases of colon. J. Clin. Pathol. *40*, 312–317.

Miyoshi, H., and Stappenbeck, T.S. (2013). *In vitro* expansion and genetic modification of gastrointestinal stem cells in spheroid culture. Nat. Protoc. *8*, 2471–2482.

Paludan, C., Schmid, D., Landthaler, M., Vockerodt, M., Kube, D., Tuschl, T., and Münz, C. (2005). Endogenous MHC class II processing of a viral nuclear antigen after autophagy. Science *307*, 593–596.

Pidala, J., Beato, F., Kim, J., Betts, B., Jim, H., Sagatys, E., Levine, J.E., Ferrara, J.L.M., Ozbek, U., Ayala, E., et al. (2018). *In vivo* IL-12/IL-23p40 neutralization blocks Th1/Th17 response after allogeneic hematopoietic cell transplantation. Haematologica *103*, 531–539.

Robinson, M.D., McCarthy, D.J., and Smyth, G.K. (2010). edgeR: a Bioconductor package for differential expression analysis of digital gene expression data. Bioinformatics *26*, 139–140.

Roche, P.A., and Furuta, K. (2015). The ins and outs of MHC class II-mediated antigen processing and presentation. Nat. Rev. Immunol. *15*, 203–216.

Rowe, V., Banovic, T., MacDonald, K.P., Kuns, R., Don, A.L., Morris, E.S., Burman, A.C., Bofinger, H.M., Clouston, A.D., and Hill, G.R. (2006). Host B cells produce IL-10 following TBI and attenuate acute GVHD after allogeneic bone marrow transplantation. Blood *108*, 2485–2492.

Saada, J.I., Pinchuk, I.V., Barrera, C.A., Adegboyega, P.A., Suarez, G., Mifflin, R.C., Di Mari, J.F., Reyes, V.E., and Powell, D.W. (2006). Subepithelial myofibroblasts are novel nonprofessional APCs in the human colonic mucosa. J. Immunol. *177*, 5968–5979.

Shan, M., Gentile, M., Yeiser, J.R., Walland, A.C., Bornstein, V.U., Chen, K., He, B., Cassis, L., Bigas, A., Cols, M., et al. (2013). Mucus enhances gut homeostasis and oral tolerance by delivering immunoregulatory signals. Science *342*, 447–453.

Shlomchik, W.D., Couzens, M.S., Tang, C.B., McNiff, J., Robert, M.E., Liu, J., Shlomchik, M.J., and Emerson, S.G. (1999). Prevention of graft versus host disease by inactivation of host antigen-presenting cells. Science *285*, 412–415.

Shono, Y., Docampo, M.D., Peled, J.U., Perobelli, S.M., Velardi, E., Tsai, J.J., Slingerland, A.E., Smith, O.M., Young, L.F., Gupta, J., et al. (2016). Increased GVHD-related mortality with broad-spectrum antibiotic use after allogeneic hematopoietic stem cell transplantation in human patients and mice. Sci. Transl. Med. *8*, 339ra71.

Skoskiewicz, M.J., Colvin, R.B., Schneeberger, E.E., and Russell, P.S. (1985). Widespread and selective induction of major histocompatibility complex-determined antigens *in vivo* by gamma interferon. J. Exp. Med. *162*, 1645–1664.

Srinivas, S., Watanabe, T., Lin, C.S., William, C.M., Tanabe, Y., Jessell, T.M., and Costantini, F. (2001). Cre reporter strains produced by targeted insertion of EYFP and ECFP into the ROSA26 locus. BMC Dev. Biol. *1*.

Stevanovic, S., van Bergen, C.A., van Luxemburg-Heijs, S.A., van der Zouwen, B., Jordanova, E.S., Kruisselbrink, A.B., van de Meent, M., Harskamp, J.C., Claas, F.H., Marijt, E.W., et al. (2013). HLA class II upregulation during viral infection leads to HLA-DP-directed graft-versus-host disease after CD4+ donor lymphocyte infusion. Blood *122*, 1963–1973.

Teshima, T., Ordemann, R., Reddy, P., Gagin, S., Liu, C., Cooke, K.R., and Ferrara, J.L. (2002). Acute graft-versus-host disease does not require alloantigen expression on host epithelium. Nat. Med. *8*, 575–581.

Thelemann, C., Eren, R.O., Coutaz, M., Brasseit, J., Bouzourene, H., Rosa, M., Duval, A., Lavanchy, C., Mack, V., Mueller, C., et al. (2014). Interferon-γ induces expression of MHC class II on intestinal epithelial cells and protects mice from colitis. PLoS ONE *9*, e86844.

Toubai, T., Tawara, I., Sun, Y., Liu, C., Nieves, E., Evers, R., Friedman, T., Korngold, R., and Reddy, P. (2012). Induction of acute GVHD by sex-mismatched H-Y antigens in the absence of functional radiosensitive host hematopoietic-derived antigen-presenting cells. Blood *119*, 3844–3853.

Unanue, E.R., Turk, V., and Neefjes, J. (2016). Variations in MHC Class II Antigen Processing and Presentation in Health and Disease. Annu. Rev. Immunol. *34*, 265–297.

Varelias, A., Gartlan, K.H., Kreijveld, E., Olver, S.D., Lor, M., Kuns, R.D., Lineburg, K.E., Teal, B.E., Raffelt, N.C., Cheong, M., et al. (2015). Lung parenchyma-derived IL-6 promotes IL-17A-dependent acute lung injury after allogeneic stem cell transplantation. Blood *125*, 2435–2444.

Varelias, A., Ormerod, K.L., Bunting, M.D., Koyama, M., Gartlan, K.H., Kuns, R.D., Lachner, N., Locke, K.R., Lim, C.Y., Henden, A.S., et al. (2017). Acute graft-versus-host disease is regulated by an IL-17-sensitive microbiome. Blood *129*, 2172–2185.

Vatanen, T., Kostic, A.D., d'Hennezel, E., Siljander, H., Franzosa, E.A., Yassour, M., Kolde, R., Vlamakis, H., Arthur, T.D., Hämäläinen, A.M., et al.; DIABIMMUNE Study Group (2016). Variation in Microbiome LPS Immunogenicity Contributes to Autoimmunity in Humans. Cell *165*, 842–853.

Vossen, J.M., Heidt, P.J., van den Berg, H., Gerritsen, E.J., Hermans, J., and Dooren, L.J. (1990). Prevention of infection and graft-versus-host disease by suppression of intestinal microflora in children treated with allogeneic bone marrow transplantation. Eur. J. Clin. Microbiol. Infect. Dis. *9*, 14–23.

Weizman, O.E., Adams, N.M., Schuster, I.S., Krishna, C., Pritykin, Y., Lau, C., Degli-Esposti, M.A., Leslie, C.S., Sun, J.C., and O'Sullivan, T.E. (2017). ILC1 Confer Early Host Protection at Initial Sites of Viral Infection. Cell *171*, 795–808.e12.

Yamamoto, M., Sato, S., Hemmi, H., Hoshino, K., Kaisho, T., Sanjo, H., Takeuchi, O., Sugiyama, M., Okabe, M., Takeda, K., and Akira, S. (2003). Role of adaptor TRIF in the MyD88-independent toll-like receptor signaling pathway. Science *301*, 640–643.

Zeiser, R., and Blazar, B.R. (2017). Acute Graft-versus-Host Disease—Biologic Process, Prevention, and Therapy. N. Engl. J. Med. *377*, 2167–2179.

Zhang, P., Lee, J.S., Gartlan, K.H., Schuster, I.S., Comerford, I., Varelias, A., Ullah, M.A., Vuckovic, S., Koyama, M., Kuns, R.D., et al. (2017). Eomesodermin promotes the development of type 1 regulatory T (TR1) cells. Sci. Immunol. *2*, eaah7152.

STAR★METHODS

KEY RESOURCES TABLE

REAGENT or RESOURCE	SOURCE	IDENTIFIER
Antibodies		
Alexa Fluor 700 anti-mouse CD45.2	BioLegend	Cat# 109822, RRID AB_493731
FITC anti-mouse CD45.2	BioLegend	Cat# 109806, RRID AB_313443
PE anti-mouse CD31	BioLegend	Cat# 102408, RRID AB_312903
APC anti-mouse TER-119	BioLegend	Cat# 116212, RRID AB_313713
Pacific Blue anti-mouse I-A/I-E	BioLegend	Cat# 107620, RRID AB_493527
Pacific Blue anti-mouse CD69	BioLegend	Cat# 104524, RRID AB_2074979
Alexa Fluor 647 anti-mouse CD326 (EpCAM)	BioLegend	Cat# 118212, RRID AB_1134101
PE-CF594 Rat Anti-Mouse CD19	BD Biosciences	Cat# 562291, RRID AB_11154223
BV650 Hamster Anti-Mouse CD3	BD Biosciences	Cat# 564378, RRID AB_2738779
BV711 Hamster Anti-Mouse CD3	BD Biosciences	Cat# 563123, RRID AB_2687954
PerCP/Cyanine5.5 anti-mouse TCRβ	BioLegend	Cat# 109228, RRID AB_1575173
Brilliant Violet 421 anti-mouse TCRγδ	BioLegend	Cat# 118119, RRID AB_10896753
PerCP-Cy5.5 Rat Anti-Mouse CD4	BD Biosciences	Cat# 550944, RRID AB_393977
BV711 Rat Anti-Mouse CD8a	BioLegend	Cat# 563046, RRID AB_2737972
PE/Cy7 anti-mouse CD335 (NKp46)	BioLegend	Cat# 137618, RRID AB_11219186
APC/Cy7 anti-mouse Ly-6G	BioLegend	Cat# 127624, RRID AB_10640819
Brilliant Violet 605 anti-mouse CD11c	BioLegend	Cat# 117334, RRID AB_2562415
PE/Cy7 anti-mouse CD64 (FcγRI)	BioLegend	Cat# 139314, RRID AB_2563904
PerCP/Cyanine5.5 anti-mouse/human CD11b	BioLegend	Cat# 101228, RRID AB_893232
PE anti-mouse CD40	BioLegend	Cat# 124610, RRID AB_1134075
PE anti-mouse CD80	BioLegend	Cat# 104708, RRID AB_313129
PE anti-mouse CD86	BioLegend	Cat# 105008, RRID AB_313151
PE Rat IgG2a, κ Isotype control	BioLegend	Cat# 400508, RRID AB_326530
PE Armenian Hamster IgG Isotype control	BioLegend	Cat# 400908, RRID AB_326593
Pacific Blue Rat IgG2b, κ Isotype control	BioLegend	Cat# 400627, RRID AB_493561
Alexa Fluor 647 anti-T-bet	BioLegend	Cat# 644804, RRID AB_1595466
Alexa Fluor 647 Mouse IgG1, κ Isotype control	BioLegend	Cat# 400136
CD90.1 Monoclonal Antibody (HIS51), APC-eFluor 780	eBioscience	Cat# 47-0900-82, RRID AB_1272252
CD200 Receptor Monoclonal Antibody (OX110), APC	eBioscience	Cat# 17-5201-82, RRID AB_10717289
APC Rat IgG2a, κ Isotype control	BioLegend	Cat# 400512
FITC Rat Anti-Mouse Vβ 6 T Cell Receptor	BD Biosciences	Cat# 553193, RRID AB_394700
Biotin Rat Anti-Mouse CD49b (DX5)	BD Biosciences	Cat# 553856, RRID AB_395092
BV421 Mouse Anti-Mouse NK1.1	BD Biosciences	Cat# 562921, RRID AB_2728688
Alexa Fluor® 700 anti-mouse Ly-6C	BD Biosciences	Cat# 128024, RRID AB_10643270
CD119 (IFN γ Receptor 1) Monoclonal Antibody (2E2), PE	BD Biosciences	Cat# 12-1191-82, RRID AB_1210730
BV786 Streptavidin	BD Biosciences	Cat# 563858
Recombinant Anti-Villin antibody [SP145]	Abcam	Cat# ab130751
Rabbit IgG, monoclonal [EPR25A] - Isotype Control	Abcam	Cat# ab172730
Goat Anti-Rabbit IgG H&L (Alexa Fluor® 555)	Abcam	Cat# ab150086
Alexa Fluor 647 Rabbit monoclonal Anti-Vimentin antibody [EPR3776]	Abcam	Cat# ab194719
Alexa Fluor 647-Rabbit IgG, monoclonal [EPR25A] - Isotype Control	Abcam	Cat# ab199093
Anti-Alpha-Smooth Muscle Actin eFluor 660	eBioscience	Cat# 50-9760

(*Continued on next page*)

Continued

REAGENT or RESOURCE	SOURCE	IDENTIFIER
Mouse IgG2a, K Isotype Control eFluor 660	eBioscience	Cat# 50-4727
LIVE/DEAD Fixable Aqua Dead Cell Stain Kit	ThermoFisher	Cat# L34957
Alexa Fluor® 647 anti-mouse CD45	BioLegend	Cat# 103124, RRID AB_493533
Alexa Fluor® 647 Rat IgG2b, κ Isotype control	BioLegend	Cat# 400626, RRID AB_389343
PE anti-mouse I-A/I-E	BioLegend	Cat# 107608, RRID AB_313323
PE Rat IgG2b, κ Isotype control	BioLegend	Cat# 400636, RRID AB_893669
Anti-HLA DR+DP+DQ antibody [WR18] PE	Abcam	Cat# Ab23901
PE Mouse IgG2a, κ Isotype control	BioLegend	Cat# 400244
Alexa Fluor 647 anti-human CD45	BioLegend	Cat# 304018, RRID AB_389336
Alexa Fluor 647 Mouse IgG1, κ Isotype control	BioLegend	Cat# 400130, RRID AB_2800436
Alexa Fluor 488 anti-human CD326 (EpCAM)	BioLegend	Cat# 324210, RRID AB_756084
Alexa Fluor 488 Mouse IgG2b, k isotype control	BioLegend	Cat# 400329
LEAF Purified anti-mouse CD80	BioLegend	Cat# 104710, RRID AB_313131
Ultra-LEAF Purified Armenian Hamster IgG Isotype control	BioLegend	Cat# 400940, RRID AB_11203529
Purified CD4 (clone GK1.5)	ATCC	TIB-207
Purified CD8β (clone 53-5.8)	QIMR Berghofer	N/A
Purified CD25 (clone PC-61.5.3)	ATCC	TIB-222
Biological Samples		
Human duodenal tissue from healthy donors	Mater Inflammatory Bowel Disease (IBD) Biobank, Mater Research Institute	N/A
Chemicals, Peptides, and Recombinant Proteins		
Recombinant Human IFN-γ	BioLegend	Cat# 570204
D-Luciferin	Perkin Elmer	Cat# 122799
Recombinant Human IL-2 (Proleukin)	Novartis	N/A
7-Aminoactinomycin D (7AAD)	Sigma Aldrich	Cat# A9400-5MG
Phorbol 12-myristate 13-acetate (PMA)	Sigma Aldrich	Cat#P1585-1MG
Ionomycin	Sigma Aldrich	Cat#I0634-1MG
Brefeldin A Solution (1000X)	BioLegend	Cat#420601
Carboxyfluorescein succinimidyl ester (CFSE)	Sigma Aldrich	Cat#21888-25MG-F
Cultex PathClear Reduced Growth Factor BME	R&D Systems	Cat#RDS353301002
SB431542	Selleck Chemicals	Cat#S1067-50mg
Y-27532 dihydrochloride	Tocris Bioscience	Cat#RDS125410
G418 disulfate salt solution	Sigma Aldrich	Cat#G8168-10ML
Hygromycin B Gold	Invivogen	Cat#ant-hg-1
Ethylenediaminetetraacetic Acid Disodium	Chem-supply	CAS#6381-92-6
Trypsin 2.5%	Thermo Fisher	Cat#15090-046
Tamoxifen	MP Biomedicals	CAS#10540-29-1
Critical Commercial Assays		
BD Cytofix/Cytoperm	BD Biosciences	Cat# 554714
Fixation/Permeabilization Kit		
eBioscience Foxp3 / Transcription Factor Staining Buffer Set	eBioscience	Cat# 00-5523-00
Cytometric Bead Array; IFNγ, IL-6, TNF, IL-17A	BD Biosciences	Cat#560485
Lamina Propria Dissociation Kit, mouse	MACS Miltenyi Biotec	Cat#130-097-410
RNeasy Mini Kit	QIAGEN	Cat# 74106
TruSeq Stranded Total RNA Ribo-Zero GOLD	Illumina	Cat#RS-122
NextSeq 75 cycle High output run	Illumina	Cat#FC-404-1005

(*Continued on next page*)

Continued

REAGENT or RESOURCE	SOURCE	IDENTIFIER
Deposited Data		
Raw RNaseq data	European Nucleotide Archive	PRJEB33777, https://www.ebi.ac.uk/ena
Experimental Models: Cell Lines		
L-WRN (ATCC CRL-3276)	ATCC	Cat#CRL-3276; RRID:CVCL_DA06
Experimental Models: Organisms/Strains		
Mouse: B6.WT: C57BL/6JArc	The Animal Resources Centre (ARC), Perth, AU	N/A
Mouse: BALB/c: BALB/cArc	ARC	N/A
Mouse: B6D2F1: B6D2F1J/Arc	ARC	N/A
Mouse: B6.*Rag*$^{-/-}$: *Rag1*$^{-/-}$	QIMR Berghofer	N/A
Mouse: B6.*Rag*$^{-/-}$*Il2rg*$^{-/-}$: *Rag2*$^{-/-}$*Il2rg*$^{-/-}$	QIMR Berghofer	N/A
Mouse: B6.*I-A*$^{b-/-}$: *H2-Ab*$^{-/-}$	Australian National University, Canberra, AU	Grusby et al., 1991
Mouse: *Villin* Cre-ER^{T2}	Dr R Blumberg, Harvard Medical School, Boston, MA, USA	el Marjou et al., 2004
Mouse: *Rosa26*-YFP	Dr B. Stockinger, MRC National Institute for Medical Research, Mill Hill, London, UK	Srinivas et al., 2001
Mouse: B6 $^{luc+:}$ *β-actin*-luciferase C57BL6J	Dr Robert Negrin, Stanford, CA, USA	N/A
Mouse: BALB/c $^{luc+:}$ *β-actin*-luciferase BALB/c	Dr Robert Negrin, Stanford, CA, USA	N/A
Mouse: Marilyn Tg (*Rag2*$^{-/-}$ background)	Dr P Matzinger, NIH, Bethesda, MD, USA	N/A
Mouse: B6.*I-A*^{b}*β*-GFP: *I-A*^{b}*β*-EGFP	Dr Barbara Fazekas de St Groth, Garvan Institute, Sydney, AU	Boes et al., 2002
Mouse: B6.*Myd88*$^{-/-}$*Trif*$^{-/-}$	Dr S Akira, Osaka University, Osaka, Japan	N/A
Mouse: B6.*il17ra*$^{-/-}$: *il17ra*$^{-/-}$	Amgen	N/A
Mouse: *I-A*$^{b\text{-}fl/fl}$: B6.129X1-*H2-Ab1tm1Koni*/J	The Jackson Laboratory	013081
Mouse: *Villin*-Cre: B6.SJL-*Tg(Vil-cre)997Gum*/J	The Jackson Laboratory	004586
Mouse: *Nestin*-Cre: B6.Cg-*Tg(Nes-cre)1Kln*/J	The Jackson Laboratory	003771
Mouse: *Tie2*-Cre: B6.Cg-*Tg(Tek-cre)1Ywa*/J	The Jackson Laboratory	008863
Mouse: B6.*Il12/23p40*-YFP: B6.129-*Il12btm1Lky*/J	The Jackson Laboratory	006412
Mouse: B6.*Ifnγ*-YFP: B6.129S4-*Ifngtm3.1Lky*/J	The Jackson Laboratory	017581
Mouse: B6.*Ifngr*$^{-/-}$: B6.129S7-*Ifngr1tm1Agt*/J	The Jackson Laboratory	003288
Mouse: B6.*Il12p35*$^{-/-}$: B6.129S1-*Il12atm1Jm*/J	The Jackson Laboratory	002692
Mouse: Marilyn^{luc+}: *Rag2*$^{-/-}$ Marilyn mice were backcrossed onto a B6 β-actin-luciferase background	QIMR Berghofer	N/A
Each of the Cre strain and I-A$^{b\ -fl/fl}$ or *Rosa26*-YFP strains were intercrossed to generate:		N/A
Mouse: *Villin*-Cre $^{I\text{-}Ab\text{-}fl/fl}$	QIMR Berghofer	N/A
Mouse: *Villin*-Cre-ER^{T2} *I-A*$^{b\text{-}fl/fl}$	QIMR Berghofer	N/A
Mouse: *Nestin*-Cre *I-A*$^{b\text{-}fl/fl}$	QIMR Berghofer	N/A
Mouse: *Tie2*-Cre *I-A*$^{b\text{-}fl/fl}$	QIMR Berghofer	N/A
Mouse: *Villin*-Cre *Rosa26*-YFP	QIMR Berghofer	N/A
Mouse: *Nestin*-Cre *Rosa26*-YFP	QIMR Berghofer	N/A
Mouse: *Tie2*-Cre *Rosa26*-YFP	QIMR Berghofer	N/A

(*Continued on next page*)

Continued

REAGENT or RESOURCE	SOURCE	IDENTIFIER
Software and Algorithms		
BD FACSDiva software version 8	BD Bioscience	https://www.bdbiosciences.com/in/instruments/software/facsdiva/
FlowJo v9	Tree Star	https://www.flowjo.com/
Zen software	Zeiss	https://www.zeiss.com/microscopy/int/downloads/brochure-downloads.html?filter=en_de%7E00012806
ImageJ 1.51w	NIH	https://imagej.nih.gov/ij/docs/intro.html
Cutadapt	Martin, 2011	https://github.com/marcelm/cutadapt
STAR	Dobin et al., 2013	https://github.com/alexdobin/STAR
EdgeR	Robinson et al., 2010; Bioconductor 3.9	http://bioconductor.org/packages/release/bioc/html/edgeR.html
GSEA	Broad Institute	http://software.broadinstitute.org/gsea/index.jsp
GraphPad Prism (ver. 7.02)	GraphPad Software	https://www.graphpad.com/scientific-software/prism/
Other		
BD LSRFortessa	BD Bioscience	https://www.bdbiosciences.com/in/instruments/lsr/index.jsp
Xenogen IVIS 100	Caliper Life Sciences	https://www.perkinelmer.com/product/ivis-spectrum-imaging-system-120v-124262
Zeiss 780-NLO Point Scanning Confocal Microscope	Zeiss	https://www.zeiss.com/microscopy/int/service-support/glossary/nlo.html
Olympus BX51 microscope	Olympus	https://www.olympus-lifescience.com/en/microscope-resource/primer/java/lightpaths/bx51fluorescence/

LEAD CONTACT AND MATERIALS AVAILABILITY

Further information and requests for resources and reagents should be directed to and will be fulfilled by the Lead Contact, Geoffrey R. Hill (grhill@fredhutch.org).

EXPERIMENTAL MODEL AND SUBJECT DETAILS

Mice

C57BL/6J (B6.WT, H-2^{b}, CD45.2^{+}), BALB/c (H-2^{d}, CD45.2^{+}) and B6D2F1 (H-2$^{b/d}$, CD45.2^{+}) were purchased from the Animal Resources Centre, Perth, AUS. B6.*Rag1*$^{-/-}$ and B6.*Rag2*$^{-/-}$*Il2rg*$^{-/-}$ mice were obtained from the QIMR Berghofer animal facility. Transgenic and knockout mice on a B6 background originated as follows: *H2-A*^{b}*1*$^{-/-}$, referred to as B6.*I-A*$^{b-/-}$, Australian National University, Canberra, AU; *Villin*Cre-ER^{T2}, Dr R Blumberg, Harvard Medical School, Boston, MA, USA (Adolph et al., 2013; el Marjou et al., 2004); *Rosa26*-YFP, Dr B. Stockinger, MRC National Institute for Medical Research, Mill Hill, London, UK (Hirota et al., 2011); β-*actin*-luciferase C57BL6 and BALB/c, Dr Robert Negrin, Stanford, CA, USA (Beilhack et al., 2005); Marilyn Tg (*Rag2*$^{-/-}$ background), Dr P Matzinger, NIH, Bethesda, MD, USA (Lantz et al., 2000); B6. *I-A*$^{b}\beta$-GFP, Dr Barbara Fazekas de St Groth, Garvan Institute, Sydney, AU; 2011); B6.*MyD88*$^{-/-}$*Trif*$^{-/-}$, Dr S Akira, Osaka University, Osaka, Japan (Yamamoto et al., 2003); B6.*Il17ra*$^{-/-}$ as previously described (Varelias et al., 2017); *I-A*$^{b\text{-fl/fl}}$ (Stock 013181, B6.129X1-*H2-Ab1*^{tm1Koni}/J) (Hashimoto et al., 2002), *Villin*-Cre (Stock 004586, B6.SJL-*Tg(Vil-cre)997Gum*/J), *Nestin*-Cre (Stock 003771, B6.Cg-*Tg(Nes-cre)1Kln*/J), *Tie2*-Cre (Stock 008863, B6.Cg-*Tg(Tek-cre)1Ywa*/J), B6.*Il12/23p40*-YFP (Stock 006412, B6.129-*Il12b*^{tm1Lky}/J), B6.*Ifn*γ-YFP (Stock 017581, B6.129S4-*Ifng*$^{tm3.1Lky}$/J), B6.*Ifn*$\gamma r^{-/-}$ (Stock 003288, B6.129S7-*Ifngr1*^{tm1Agt}/J) and *IL-12p35*$^{-/-}$ (Stock 002692, B6.129S1-*Il12a*^{tm1Jm}/J), the Jackson Laboratory, Bar Harbor, MA, USA. *Rag2*$^{-/-}$ background Marilyn mice were backcrossed onto a B6 β-*actin*-luciferase background (Marilyn^{luc+}, CD90.1^{+} CD45.2^{+}). Each of the Cre strains and *I-A*$^{b\text{-fl/fl}}$ or *Rosa26*-YFP strains were intercrossed to generate *Villin*Cre *I-A*$^{b\text{-fl/fl}}$, *Villin*Cre-ER^{T2}*I-A*$^{b\text{-fl/fl}}$, *Nestin*Cre *I-A*$^{b\text{-fl/fl}}$, *Tie2*Cre *I-A*$^{b\text{-fl/fl}}$, *Villin*Cre *Rosa26*-YFP, *Nestin*Cre *Rosa26*-YFP and *Tie2*Cre *Rosa26*-YFP mice. Mice were bred at the QIMR Berghofer animal facility. B6.WT mice were housed under germ free conditions at the University of Queensland Biological Resources Facility (UQBRF). For cohousing experiments, mice were housed as described previously (Varelias et al., 2017). Mice were housed in sterilized microisolator cages and received acidified autoclaved water (pH 2.5) after transplantation. Experiments were performed with sex and age-matched animals using littermates where possible.

Stem Cell Transplantation

B6 or B6D2F1 mice were transplanted as described previously (Koyama et al., 2011) with 1000 cGy or 1100 cGy total body irradiation (TBI, 137Cs source at 84 cGy/min) on day −1, respectively. On day 0, B6 mice were transplanted with 5 × 10^6 bone marrow (BM) cells and (0.025 - 0.5 × 10^6) luciferase-expressing Marilyn cells. BM cells were depleted of T cells by antibody and complement as previously described (T cell depletion = TCD). Marilyn CD4$^+$ T cells (*Rag2*$^{-/-}$ background) were purified to greater than 98% by sorting of Vβ6$^+$ CD8^{neg} cells using a MoFlo (Beckman Coulter) or 70% by CD4 MACS system (Miltenyi). To generate MHC-II deficient BM chimeric mice, the relevant lethally irradiated Cre-^{neg}*I-A*$^{b\text{-}fl/fl}$ and Cre-^{pos}*I-A*$^{b\text{-}fl/fl}$ mice were injected with 10 × 10^6 female B6.*I-A*$^{b-/-}$ BM and treated with anti-CD4 (GK1.5) and CD8 (53-5.8) mAbs. The Abs were administrated i.p. from day −2 (GK1.5; 500 μg/ animal, 53-5.8; 150 μg/ animal) followed by weekly injection (GK1.5; 250 μg/ animal, 53-5.8; 150 μg/animal) until week 6 to prevent any persistence of recipient T cells in a class II negative environment. Five weeks after Ab discontinuation, the BM chimeric mice were used in secondary transplants. For BMT utilizing WT polyclonal CD4$^+$ T cells, lethally irradiated female mice were transplanted with 5 × 10^6 BM and 5 × 10^6 CD4$^+$ T cells (MACS purified) from Treg-depleted BALB/c donor mice (PC61; 500 μg/ animal, day −3 and −1, i.p.). Tamoxifen (1mg/day) was administered for 5 days, 2 weeks before transplant where indicated. IL-12p40 (C17.8) or control rat IgG2a (MAC4) was administered intraperitoneally at 500 μg per dose on days −2 and −1 prior to TBI, and on the day of transplant (d0) prior to the infusion of graft (BM and T cells). In BMT using B6D2F1 recipients, lethally irradiated female B6D2F1 mice were transplanted with 5 × 10^6 BM and 2 × 10^6 T cells from B6.WT mice using magnetic bead depletion as previously described (MacDonald et al., 2010). Animal procedures were undertaken using protocols approved by the institutional (QIMR Berghofer) animal ethics committee. The severity of systemic GVHD was assessed by scoring as previously described (maximum index = 10) (Cooke et al., 1996). For survival experiments, transplanted mice were monitored daily and those with GVHD clinical scores ≥ 6 were sacrificed and the date of death registered as the next day, in accordance with institutional guidelines.

METHOD DETAILS

Cell isolation from small intestine and colon

Longitudinally sectioned pieces of the small intestine or the colon were processed using a gentleMACS Dissociator and mouse lamina propria dissociation kit (both Miltenyi Biotec), according to the manufacturer's protocol. Dithiothreitol was excluded from the entire process. We sectioned the small intestine into the proximal third (duodenum), the middle third (jejunum) and the distal third (ileum).

Gut decontamination

For microflora depletion, an antibiotic cocktail of vancomycin, metronidazole, cefoxitin and gentamicin (final concentrations 1 mg/ml each) was added to the drinking water for 14 days before TBI (Hülsdünker et al., 2018). Control mice received acidified water (pH 2.5) without antibiotics.

Mouse and human organoid isolation and growth protocol

The small intestine was isolated from naive WT.B6 and B6.*I-A*^{b}β-GFP reporter mice. After rinsing with HBSS without Ca and Mg, the small intestine was cut into 1mm pieces and incubated for 15 minutes in dissociation buffer consisting of PBS and 0.02M EDTA. After physical separation, crypts were counted on a hemocytometer with trypan blue and 200 viable crypts per well were suspended in 50% type 2, PathClear Cultrex® reduced growth factor basement membrane extract. After the basement membrane was set at 38°C, 500μL of 50% conditioned media derived from the L-WRN cell line, and including ALK5 kinase inhibitor and p160ROCK inhibitor, was added to each well and grown at 38°C (Miyoshi and Stappenbeck, 2013). Growing enteroids were enumerated at day 5 with media changed every 2-3 days. 10ng/mL of recombinant murine IFNγ or diluent was added to growth media for 24 hours prior to isolation and staining for confocal microscopy. Live organoids were stained with DAPI (1/1000) and BioLegend AF647 anti-mouse CD326 (Ep-CAM). Human intestinal organoids from the duodenal tissue of 3 healthy donors were generated by the same method as above and stained with PE-conjugated anti-HLA DR+DP+DQ (Abcam), CD45 AF647 and CD326 AF488 (BioLegend) for flow cytometric analysis. The procedures were undertaken using protocols approved by the University of Queensland ethics committee.

Flow cytometry

For surface staining, cell suspensions were incubated with anti-CD16/CD32 (2.4G2) followed by staining with antibodies against CD45.2, CD31, Ter119, MHC class II (I-A/I-E), CD69, CD326 (EpCAM), CD19, CD3, TCRβ, TCRγδ, CD4, CD8, NKp46, Ly6G, CD11c, CD64, CD11b, CD40, CD80, CD86, Rat IgG2a isotype control, Armenian Hamster IgG isotype control, Rat IgG2b isotype control and T-bet (all BioLegend); CD90.1, YAe and CD200r (eBioscience); Vβ6, CD19, DX5 (CD49b), NK1.1, Ly6C and IFNγR1 (CD119) (BD Biosciences). 7AAD (Sigma) was added before cell acquisition. For intracytoplasmic staining (villin and vimentin (Abcam, Cambridge, UK) and αSMA (eBioscience)), single-cell suspensions were incubated with fixable live/dead cell dye (ThermoFisher), FcγR blocked with 2.4G2 and stained for surface markers. Cells were then fixed and permeabilized using the BD Fix/Perm kit (BD) according to the manufacturer's protocol and stained with Abs against villin, vimentin or αSMA for 30 min at room temperature, washed and acquired. T-bet expression was determined using the Foxp3 staining buffer set (eBioscience) according to the manufacturer's protocol. Samples were acquired with a BD LSRFortessa (BD) and analysis was performed with FlowJo v9 (Tree Star) software. Representative flow cytometry plots display concatenated replicates from one experiment.

Histologic analysis

H&E stained sections of formalin-fixed tissue were coded and examined in a blinded fashion by A.D.C. using a semiquantitative scoring system, as previously described (Koyama et al., 2011). Images of GVHD target tissues were acquired using an Olympus BX51 microscope (Olympus), an Evolution MP 5.0 Camera, and Qcapture software (Qimaging).

Immunofluorescence microscopy

Tissues were fixed with 4% paraformaldehyde, then placed in 30% sucrose prior to being frozen in Tissue-Tek OCT compound (Sakura Finetek). Sections (7 μm thickness) were treated with Background Sniper (Biocare Medical) and 2% BSA for 30 min and then stained with IA/IE PE (isotype Rat IgG2b PE) and CD45-Alexa flour 647 (isotype Rat IgG2b AF647) (all mAbs; BioLegend) for 120 min at room temperature in the dark. After washing, sections were counterstained with DAPI for 5 min and coverslipped with Vector Vectashield Hard Set mounting media. Samples for quantitation of mucus thickness were prepared as described (Johansson et al., 2008). In brief, samples were fixed in Methacarn solution (60% methanol, 30% chloroform, 10% glacial acetic acid, Sigma) for 6*h*, washed in methanol followed by ethanol and xylol, and embedded in paraffin. Slides were deparaffinized and washed in ethanol. *In situ* hybridization was performed at 46°C for 16*h* in a hybridization buffer (0.9 M NaCl, 20 mM Tris/HCl, 0.01% sodium dodecyl sulfate (SDS), 20% formamide) containing a eubacterial probe Eub338 (Cy3-GCTGCCTCCCGTAGGAGT) and non-Eub (6-FAM-ACTCCTACGGGAGGCAGC) (each 10ng/μl). Slides were washed in washing buffer (0.225 M NaCl, 20 mM Tris/HCl, 0.01% SDS, 5 mM EDTA) for 15 min, then in PBS and blocked in PBS containing 4% FCS. Polyclonal Muc2 antibody was applied for 4-16*h* at 4°C followed by incubation with secondary anti-rabbit Alexa Fluor 647 antibody for 1-2*h* at 4°C and DAPI for counterstaining. Images were taken with x40 oil-immersion lens or x10 non-oil lens using a Zeiss 780-NLO Point Scanning Confocal Microscope with Zen software (Zen software). For quantification of MHC-II expression by IEC, mean fluorescence intensity (MFI) was measured with ImageJ 1.51w software, whereby each data point represents the average from the epithelial layer of 9-15 villi from 3-5 high-power fields per animal, standardized to expression within naive WT (Figures 3, 4, and 7) or MHC-II-GFP (Figure 1) animals (fold-change).

Mixed lymphocyte reaction (MLR)

Carboxy fluorescein diacetate succinimidyl ester (CFSE) labeling was performed as described (Koyama et al., 2015). In round-bottom 96-well plates, sort-purified CFSE-labeled Marilyn^{luc+} cells (CD90.1^{+}) were stimulated with sort-purified intestinal epithelial cells (IEC) (CD326^{+}CD45.2^{neg}) from the small intestine of female or male B6.WT mice which had undergone TBI 20*h* before, in the presence of rhIL-2 (100 U/ml) (Zhang et al., 2017). Seven days later, Marilyn^{luc+} T cells (CD90.1^{+}CD4^{+}CD45.2^{+}) were assessed for CFSE dilution and expression of CD69 by flow cytometry. For CD80 blocking, purified CD80 mAb (clone 16-10A1, BioLegend) or its isotype control (Armenian Hamster IgG, BioLegend) was added to cultures at 1 μg / ml.

Cytokine analysis

Serum TNF levels were determined using the BD Cytometric Bead Array system (BD Biosciences PharMingen) according to the manufacturer's protocol.

Bioluminescence imaging (BLI)

T cell expansion was determined by analysis of luciferase signal intensity (Xenogen IVIS 100; Caliper Life Sciences). Light emission is presented as photons per second per square centimeter per steer radiant (ph/s/cm2/sr). Total flux of mouse or organ is presented as photons per second (ph/s). Mice were subcutaneously injected with 500 μg d-Luciferin (PerkinElmer) and imaged 5 min later (Koyama et al., 2011).

RNA sequencing

Total RNA was extracted from sort-purified IEC (CD45^{neg}*Villin*-YFP^{+} 7AAD^{neg}) from *Villin*Cre^{+}*Rosa26*YFP mice using the RNeasy mini kit (QIAGEN). For library preparation and sequencing, TruSeq Stranded Total RNA Ribo-Zero GOLD and NextSeq 75 cycle High output run (Illumina) were utilized, respectively. We compared IEC from naive mice, those from mice 4 days after TBI but not transplanted, those from transplanted (BALB/c → *Villin*Cre^{+}*Rosa26*YFP) non-GVHD mice (i.e., transplanted with TCD grafts) and those from GVHD mice (transplanted with T cell replete grafts). Sequence reads were trimmed for adaptor sequences using Cutadapt and aligned to the mm10 assembly using STAR aligner. The read counts per gene were estimated using RSEM and were utilized to determine differential gene expression between groups using Bioconductor package 'edgeR'. The default TMM normalization method of edgeR was used to normalize read counts between samples. Differentially expressed genes were considered significant if the Benjamini-Hochberg corrected p value was less than 0.01. Gene set enrichment analysis (GSEA 3.0, Broad Institute) was used to determine gene sets and pathways that are significantly enriched in up and down differentially expressed genes (fold change > 2, fdr < 0.01) for each group of comparison against the GSEA molecular signature database. The gene sets that were significant with an FDR < 0.05 and are common in all comparisons from the above GSEA analysis were utilized for single-sample GSEA (ssGSEA) analysis. ssGSEA analysis reveals the pathways that are differentially regulated between the samples. The sample projection values for each pathway from ssGSEA analysis were used to construct a heatmap demonstrating changes in pathway enrichments for each sample.

QUANTIFICATION AND STATISTICAL ANALYSIS

Data were analyzed using GraphPad Prism (ver. 7.02). Survival curves were plotted using Kaplan-Meier estimates and compared by log-rank test. If the equality of variance tests indicated the group variances were not significantly different ($p > 0.01$) and the data was normally distributed, one-way ANOVA (Tukey's multiple comparison test) was used for multiple test comparisons or unpaired t tests (two-tailed) for two group comparisons. For data that was not normally distributed, Kruskal-Wallis test (Dunn's multiple comparison test) was used for multiple group comparisons or Mann Whitney-U tests (two-tailed) for comparisons of two groups. When comparing in multiple ways, ANOVA or Kruskal-Wallis test was used for parametric and non-parametric comparisons respectively. Data are presented as mean ± standard error of the mean (SEM).

DATA AND CODE AVAILABILITY

The accession number for the RNA sequencing data is European Nucleotide Archive: PRJEB33777.